Norwegian University
of Life Sciences

Master's Thesis 2023   30 ECTS
Faculty of Science and Technology

Exploration of the effects of neuron model properties on network dynamics

Kristoffer Hemm

Data science

Acknowledgements

I wish to thank my supervisor Prof. Dr. Hans Ekkehard Plesser for his guidance and help throughout this work. I would also like to thank Håkon Mørk and Jan-Eirik Welle Skaar for their guidance on working with the NEST Simulator and running simulations on the JUSUF system at Jülich Supercomputing Centre. To all the students at the Data Science department at NMBU, thank you for creating a good learning environment and for all the good discussions over the last couple of years. Finally, I want to thank Nissan Karki for all the collaborative work done during our time at NMBU.

Abstract

The human brain is a complex system, consisting of over 80 billion neurons and the connection between these neurons. Due to the complexity of the brain, we are still far away from successfully being able to simulate the brain in detail. With modern computational technology we must make the tradeoff between modelling the neurons in detail, at the expense of network size, or to reduce the complexity of the neuron model in order to simulate a larger network. When making simplifications in modelling neural networks, modelers have different mathematical models at their disposal. One potential challenge in computational neuroscience is that different research groups may use different models in their effort to model the same phenomenon. In this thesis we explore how using different mathematical models to model the synapse between neurons may affect the dynamics in a network of neurons. For our work we use the integrate-and-fire neuron model, where the neurons are arranged in a Brunel network. We use three different waveform functions to model the current in the synapses between neurons. These include the delta function, the alpha function, and the exponential decay function. The dynamics of the networks are explored using spiking statistics that include the firing rate, the coefficient of variation, the correlation coefficient and Wasserstein distances. We explore the dynamics in networks of different sizes and in different firing regimes, keeping all parameters fixed. Our results show that the alpha synapse model have the highest firing rate in all regimes and network sizes. The exponential decay synapse model has the lowest firing rate in all regimes and network sizes, and the firing rate of the delta synapse model fall in between. The results also give an indication the separation into clearly defined firing regimes may not be as consistent as reported by others. All three synapse models are able to clearly separate between the regular and irregular regimes, but they all display difficulty in separating the between the irregular regimes.

Contents

List of Figures

List of Tables

Chapter 1

Introduction

Modern neuroscience is a diverse scientific field, attracting researchers in scientific disciplines ranging from psychology and biology to fields like physics, mathematics, and computer science. Consisting of approximately 86 billion interconnected neurons, the human brain is one of the most complex systems currently known to mankind (Sterratt et al., 2011).

Hodgkin and Huxley's work on the squid giant axon, where they successfully modelled the generation and propagation of the action potential down the axon (Hodgkin and Huxley, 1952), is considered a landmark event in the field of computational neuroscience. Following their seminal work, considerable effort has been put into modelling the dynamics of the human brain. Descriptive models that sit at the intersection of biology and physics have shed light on how individual neurons work. However, the mechanisms underlying how the interplay between neurons give rise to complex brain function, like cognition and emotion, remain poorly understood (Wnuk et al., 2018). The frontier of modern neuroscience is to model dynamics in the brain using mechanistic models, which involve modelling the individual neurons explicitly, then connecting them to form a network. This approach is computationally demanding and modelling large networks in this fashion is not feasible. Simplifications at the neuron level are needed in order to model large networks of neurons. Thus, modelers have to make a tradeoff between modelling neurons in detail, or model larger networks of neurons. The neuron models with lower complexity does not model the morphology of the neuron in detail and reduce the neuron into a set of mathematical equations.

One popular simplified neuron model is of is the leaky integrate-and-fire neuron first described by Louis Lapicque in 1907 (Abbott, 1999). When making simplifications in modelling, researchers have a large toolbox of mathematical models to choose from in order to carry out the modelling. One challenge in the field of computational neuroscience may be that different research groups may choose different mathematical models to model the same phenomenon. Both neurons and the synaptic connections between the neurons may be modelled by a range of mathematical models, leading to different dynamics being displayed when the neurons are connected to form a network. The synapses between neurons are typically modelled using common waveform functions, including the delta function (Kanwal, 1983), the alpha function (Rall, 1967) and the exponential decay function (Sterratt et al., 2011). The goal of this thesis is to explore whether using these three different waveform functions to model the synapse affect the dynamics of a neural network.

The majority of the work draw inspiration from Brunel (2000), where the delta synapse model is used to explore dynamics of neural networks in a range of different regimes. The different regimes are mainly a function of the synaptic delay, D, the ratio of inhibitory to excitatory weights, g, and the external rate to the threshold rate, η. By varying these parameters, Brunel identified four different regimes of network dynamics, characterized by the synchronicity and regularity of neuron firing. He called them synchronous regular, asynchronous regular, asynchronous irregular, and synchronous irregular. Further, the synchronous irregular regime was divided into slow and fast oscillatory states. We explore the dynamics displayed by networks built with the different synapse models in these regimes and try to uncover any differences that the different synapse models may introduce on the dynamics in the different regimes.

Simulations are done at selected points inside each regime. In addition, simulations are done with varied values of D, g and η in order to sweep over areas within the regimes. By doing this we try to uncover whether the dynamics displayed by the different synapse models are uniform within each regime. We also explore whether we are able to clearly distinguish between the different regimes using the different synapse models. We also explore whether we can tune different neuron parameters in order to reduce potential differences the different synapse models may show. The size of a neural network has been shown to affect the dynamics of the network (Albada et al., 2015). We will also

explore how changing the size of the networks may affect dynamics of the network, and if there will be any difference in the observed dynamics when using the different synapse models. The dynamics displayed by the networks will be described using the firing rate, coefficient of variation, correlation coefficient, and Wasserstein distances.

Chapter 2

Theory

2.1 Neurons

The brain is a complex network consisting of neurons and the synaptic connections between these neurons. The primary compartments of the neurons are the soma, the axon, and the dendrites (Bloom et al., 2005). The soma, or cell body, of the neuron shares many properties with other eukaryotic cells. The soma contains the organelles of the cell, including the nucleus, containing the genetic information, and the mitochondria, responsible for producing energy required to sustain the cell. Additionally, a difference in electric potential is observed between the outside and the inside of the membrane of eukaryotic cells. This is known as a membrane potential. The major differences from other eukaryotic cells are the axon and dendrites found in neurons. The axon and the dendrites are the parts of the neuron responsible for propagating the electrochemical signal which drives the nervous system. The electrochemical signal is propagated through a neuron when its dendrites receive electrochemical signals from neighboring neurons. This leads to a change in the local membrane potential of the dendrite. The local change in membrane potential will travel to the soma of the neuron. In the soma, an electrical potential will build up caused by the incoming signals from the dendrites. If the electrical potential built up reaches a certain threshold, an action potential will be triggered in the soma. The action potential will travel down the axon in the direction of the axon terminal. The axon terminal has vesicles containing neurotransmitters. At the arrival of an action potential, the neurotransmitters

will be released into the synaptic cleft, the space between a neuron's axon and its neighboring dendrites. The neurotransmitters will bind to receptors on the dendrite of the postsynaptic neuron, leading to a change in the local membrane potential of the postsynaptic neuron. Depending on the type of neurotransmitter released by the presynaptic neuron, this change in membrane may be excitatory, increasing the likelihood of the postsynaptic neuron firing an action potential, or inhibitory, decreasing the likelihood of the postsynaptic neuron firing an action potential.

2.2 Complexity of neuron models

Neuron models generally fall into one of three categories, rate-based models, integrate-and-fire models, or mechanistic models (Sterratt et al., 2011). The mechanistic models, also known as multi-compartment models, model the morphology of neurons in detail. These models are very computationally demanding and not suitable for modelling large network models. The morphology of neurons is not modelled in detail using the integrate-and-fire model (Dayan and Abbott, 2001), or in rate-based models (Sterratt et al., 2011), making these models more suitable for simulations of large network simulations. In the integrate-and-fire model, the neuron representation is reduced to the membrane potential, V, usually modelled as an RC-circuit

$$C_m \frac{dV}{dt} = -\frac{V - E_m}{R_m} + I(t) \tag{2.1}$$

where C_m is the membrane capacitance, R_m is the membrane resistance and $I(t)$ is the total current flowing into the cell. This equation is often rewritten as

$$\tau_m \frac{dV}{dt} = -V + E_m + R_m I(t) \tag{2.2}$$

where τ_m represents the membrane time constant, given by $\tau_m = C_m R_m$. For constant input $I(t)$, the membrane potential, $V(t)$, has the solution

$$V(t) = E_m + R_m I \left(1 - exp \left(\frac{-t}{\tau_m} \right) \right). \tag{2.3}$$

If $V(t)$ reaches a threshold θ, the neuron will fire, and after a set refractory time, the membrane potential is reset to the resting potential. The total current, $I(t)$, flowing into the neuron, typically come through synapses shared with other neurons. This usually happens if the neighboring presynaptic neuron fires an action potential that travels down the axon and release neurotransmitters into the synaptic cleft.

2.3   Action potential

In a mammalian neuron, the resting membrane potential is typically around -65mV (Sterratt et al., 2011), meaning that the intracellular electric potential is lower than the electric potential outside of the neuron. The action potential refers to the sharp reversal of a neuron's electrical state, also known as a depolarization. If a depolarization event occurs, the membrane potential rapidly turns positive as positively charged ions move into the neuron and an action potential may be triggered. The depolarization is followed by a refractory period, where the neuron slowly reverts back to the resting potential. Depending on the model used for the neuron, the neuron may not be able to fire an action potential during the refractory period, or it may be more likely to fire during this period. If the buildup of electric potential in a neuron reaches the threshold required to fire, an action potential will travel down the axon in toward the synaptic terminal. Hodgkin and Huxley were the first to successfully develop a mathematical representation of the action potential (Hodgkin and Huxley, 1952).

When an action potential reaches the synaptic terminal, neurotransmitters are released into the synapse shared between two neurons. The events in the synapse may be modelled with different level of complexity.

2.4   Synapse models

There are two general approaches to model the synapses between neurons (Sterratt et al., 2011). One may take a chemical approach and model the flow of neurotransmitters from the presynaptic vesicles, across the synaptic cleft, and the chemical responses this trigger in the postsynaptic neuron. This

approach to modelling may quickly become very computationally demanding if many chemical processes are included in the model. These processes may include modelling in detail the chemical events in the presynaptic vesicles, the movement of neurotransmitters and ions, and the postsynaptic response to the neurotransmitter. To reduce the complexity of the models, one may take an electrical approach to model the events in the synapse. In an electrical model, the focus is to model the postsynaptic electrical current, $I_{syn}(t)$, resulting from an incoming spike from a neighboring neuron at a certain point in time. Here this is exemplified using the exponential decay function:

$$I_{syn}(t) = \begin{cases} \bar{I}_{syn} exp\left(-\frac{t-t_s}{\tau_{syn}}\right) & for\ t \geq t_s \\ 0 & for\ t < t_s \end{cases} \tag{2.4}$$

where $\bar{I}_{syn}$ is the maximum current possible in the synapse and t_s is the time when an incoming spike arrives.

Several waveform functions have been proposed for how to model the change in the synaptic current, $I_{syn}(t)$. These include the single exponential decay function(Sterratt et al., 2011), the alpha function (Rall, 1967) and the delta function (Kanwal, 1983)

$$I_{syn}(t) = \bar{I}_{syn} exp\left(\frac{t-t_s}{\tau}\right) \tag{2.5}$$

$$I_{syn}(t) = \bar{I}_{syn}\frac{t-t_s}{\tau} exp\left(\frac{t-t_s}{\tau}\right) \tag{2.6}$$

$$I_{syn}(t) = \bar{I}_{syn}\delta(t-\xi) \tag{2.7}$$

where $\bar{I}_{syn}$ is the maximum current possible in the synapse, $t - t_s$ is the time after the arrival of a presynaptic spike. τ is a time constant. The simplified delta function (2.7) has the following properties:

$$\delta(t-\xi) = 0, t \neq \xi \tag{2.8}$$

$$\int_a^b \delta \left(t - \xi \right) dt = \begin{cases} 0, & a, b < \xi \ or \ \xi < a, b \\ 1, & a \leq \xi \leq b \end{cases} \tag{2.9}$$

$$\int_{-\infty}^{\infty} \delta \left(t - \xi \right) dt = 1 \tag{2.10}$$

Modelling the synapse as a purely electric phenomenon is a simplification, as the electric activity observed is mainly a result of the movement on ions. But for modelling purposes this simplification is often necessary. The simplification makes both the simulations and analysis of the dynamics in the network less computationally demanding. Analyzing the dynamics of a network is done by examining different types of spiking statistics.

2.5 Statistics

When investigating the dynamics of our network simulations, three spiking statistics will be calculated, the firing rate, the coefficient of variation, and the correlation coefficient. The mean firing rate gives us an overview of the level of activity within a network (Sterratt et al., 2011). For neuron i, the firing rate, FR_i, is defined as the number of spikes per time unit.

$$FR_i = \frac{S_i}{T} \tag{2.11}$$

where S_i is the number of spikes recorded during time period T. To get the mean firing rate of the network, we calculate the firing rate of multiple neurons and calculate the mean of these neurons.

The regularity in which each individual neurons in the network is firing is given by the coefficient of variation (Gabbani and Koch, 1998). A coefficient of variation close to zero means that the firing of the neuron is highly regular. To calculate coefficient of variation, CV, we use interspike intervals, ISI, defined as the time interval between two consecutive spikes fired from a neuron. Using the interspike intervals we calculate the coefficient of variation by

$$CV = \frac{\sigma_{ISI}}{\mu_{ISI}} \tag{2.12}$$

where μ_{ISI} is the mean of the interspike intervals and σ_{ISI} is the standard deviation of the interspike intervals. To find the distribution of the coefficients of variation in the network, the coefficient of variation is calculated for multiple neurons in the network.

The regularity of the firing between neurons in the network is given by the Pearson correlation coefficient (Devore et al., 2021). The correlation coefficient tells us how closely the firing of one neuron is correlated to the firing of other neurons in the network. When considering the distribution of two firing neurons, i and j, the correlation coefficient is calculated as

$$CC_{i,j} = \frac{\sum(\mathbf{t}_i - \mu_i)(\mathbf{t}_j - \mu_j)}{\sqrt{\sum(\mathbf{t}_i - \mu_i)^2(\mathbf{t}_j - \mu_j)^2}} \tag{2.13}$$

where $\mathbf{t}_i$ and $\mathbf{t}_j$ are binned spike trains of neuron i and j, μ_i and μ_j are the mean spike counts of the binned spike trains of neuron i and j.

When reporting the statistics, the firing rate is given in spikes per second, while the coefficient of variation and correlation coefficient are unitless.

Distance metrics can be used for comparing how large the difference between two distributions is. One such distance metric is the Wasserstein distance, also known as the earth mover distance (Ramdas et al., 2017) which is given by

$$W_p(P, Q) = \left(\inf_{\pi \in \Gamma(P,Q)} \int_{\mathbb{R}^d \times \mathbb{R}^d} ||X - Y||^p d\pi \right)^{\frac{1}{p}} \tag{2.14}$$

where $\Gamma(P, Q)$ is the set of all joint probability measures on $\mathbb{R}^d \times \mathbb{R}^d$.

2.6 Brunel network

The Brunel network is composed of N intergrate-and-fire neurons, divided into two populations (Brunel, 2000). The first population consists of N_E excitatory neurons and the other population consists of N_I inhibitory neurons. The network is sparsely connected, where each neuron receives a spike input from C randomly chosen neurons in the network and C_{ext} connections from neurons

outside the network. Depolarization of a neuron is modelled by

$$\tau \dot{V}_i(t) = -V_i(t) + RI_i(t) \tag{2.15}$$

where $RI_i(t)$ represents the sum of inputs arriving from the different input synapses:

$$RI_i(t) = \tau \sum_j J_{ji} \sum_k \delta\left(t - t_j^k - D\right) \tag{2.16}$$

where J is the postsynaptic potential (PSP) amplitude arriving from the input neurons, and $\delta(t - t_j^k - D)$ represents the spikes arriving at time $t = t_j^k + D$, here shown with the delta function (Kanwal, 1983). D is the transmission delay. For simplicity, all PSP amplitudes are given the same value in each synapse, where $J_{ij} = J > 0$ in excitatory and excitatory recurrent synapses, and $J = -gJ$ in inhibitory synapses. The external synapses follow a Poisson process with rate ν_{ext}.

For simplicity, both excitatory and inhibitory neurons show the same characteristics, such as firing threshold and resting membrane potential. Another simplification is to have each neuron in the network connected to exactly the same number of inputs.

The neural spiking in the network was classified into four regimes by Brunel, synchronous regular (SR), asynchronous regular (AR), asynchronous irregular (AI) and synchronous irregular (SI), where the synchronous irregular is further separated into two states, one characterized by having slow oscillations and one characterized as having fast oscillations.

Generally, it is the firing rate that determines the synchronicity of a network. A constant firing rate over time results in an asynchronous network state with stationary global activity. If the firing rate varies over time the network state is synchronous, giving oscillating global activity.

The synchronicity of a network is dependent on the firing rate of the neurons. A constant firing rate over time lead to an asynchronous network state, giving a stationary global activity. Conversely, when the firing rate fluctuates over time the network state is in synchronous, giving an oscillating global activity. The CV statistics described above is a measure of synchronicity, where a high CV is correlated with the regimes that show a high degree of variability

in the firing rate of each neuron, leading to a low degree of synchronicity. The regularity of a network is dependent on the balance between the firing rate of excitatory and inhibitory neurons in the network. If the inhibitory neurons dominate, the network will exhibit irregular activity, and if excitatory neurons dominate, the network will exhibit regular activity.

The activity of the SR regime is described as having clusters of neurons that behave in a synchronous manner as oscillators. The regime is characterized by a high firing rate and low CV values. The activity of the AR regime is dominated by excitatory neurons with stationary global activity. A high firing rate and low CV characterize in this regime. The AI regime is described as having stationary global activity dominated by inhibitory neurons. The activity of the individual neurons is strongly irregular, and characterized by a low firing rate and a high CV. The SI regime is characterized as having oscillatory global activity and individual neurons that fire irregularly. It is characterized by a low firing rate and a high CV. In the slow state, the oscillations in the observed firing rate are slow, while in the fast SI state the oscillations in firing rate are fast.

The level of synchronicity observed in a network of neurons is dependent on the global firing rate, where a constant global firing rate over time give rise to an asynchronous network state, characterized by stationary global activity. When the global firing rate varies over time the network state is synchronous, giving oscillating global activity. The regularity is dependent on the balance between the firing rate of excitation and inhibition in the network. If inhibition dominates the network will be irregular, and if excitation dominates the network will be regular.

This means that SR is dominated by excitatory neurons which have a high degree of synchronicity, and the global network behave as oscillators. AR is dominated by excitatory neurons where individual neurons fire regularly and the global network is stationary. AI is dominated by inhibitory neurons where individual neurons fire irregularly and the global network is stationary. SI is dominated by inhibitory neurons and individual neurons fire irregularly, however the global network behaves oscillatory.

Chapter 3

Methods

3.1 NEST simulator

The data for this work is produced using the NEST simulator, version 3.4 (Sinha et al., 2023). NEST simulates the behavior of spiking neural networks

NEST is written in C++ and the simulation language SLI. All interactions with NEST are done using the PyNEST interface(Eppler et al., 2009), which makes it possible to interact with NEST using Python commands.

All simulations were run on the JUSUF supercomputer located at the Jülich research center (Mezentsev, 2020). The specifications of a standard compute node on JSUSF are given in table 3.1.

Table 3.1: JUSUF compute node

CPU	2xAMD EPYC 'Rome' 64-core processors
GPU (on selected nodes)	NVidia V100-16G GPU
RAM	16x16GB DDR4, 3200 MHz
Storage	256 GB (main memory), 1 TB NVMe device(local)
Ethernet connection	100 Gb/s HDR InfiniBand interconnect

There are two primary methods for updating the neurons in a network simulation, time-driven and event-driven (Krishnan et al., 2017). The event-driven approach utilizes a centralized event queue which determines the timing of neuron firing. When a neuron receives a spike, its state is updated and a

prediction of when it will fire is added to the central queue. NEST utilizes the time-driven scheme. In the time-driven scheme, neurons are updated on a fixed time grid. If the electric potential of a neuron passes the firing threshold at a given grid point it will fire.

3.2   Synapse models

The synapse models used in the modelling include a selection of inbuilt integrate and fire models available in NEST. These are the 'iaf_psc_alpha', 'iaf_psc_delta', and 'iaf_psc_exp' models, representing the alpha function, delta function and the exponential decay function, respectively. These models are implemented in NEST as described in (Rotter and Diesmann, 1998). The synapse models are used as implemented in NEST. In addition, the synaptic weights for the alpha synapses are normalized using the maximum of the post synaptic potential, J as the synaptic input current. This is done using the Lambert W function (Corless et al., 1996) available in NEST, equation 3.1. The implementation for updating the weights is shown in equations 3.2-5.

$$W(z)e^{W(z)} = z \tag{3.1}$$

$$a = \frac{\tau_m}{\tau_{syn}} \tag{3.2}$$

$$b = \frac{1}{\tau_{syn}} - \frac{1}{\tau_m} \tag{3.3}$$

$$t_{max} = \frac{-W\left(\frac{e^{-\frac{1}{a}}}{a}\right) - \frac{1}{a}}{b} \tag{3.4}$$

$$J = \frac{e\left(e^{-\left(\frac{t_{max}}{\tau_m}\right)} - e^{-\left(\frac{t_{max}}{\tau_{syn}}\right)}\right)}{\tau_{syn}C_m b\left(b - t_{max}e^{-\frac{t_{max}}{\tau_{syn}}}\right)} \tag{3.5}$$

Neurons in the network receive external input produced by a Poisson spike train generator. The external input is implemented using the 'poisson_generator' available in NEST.

The simulation parameters are based on Brunel's model A, where excitatory and inhibitory neurons share the same neuron properties. The networks are comprised of 10 000 excitatory neurons and 2500 inhibitory neurons, giving a 4-to-1 ratio of excitatory to inhibitory neurons in each network. The postsynaptic potentials (PSP) are set to the same amplitude, J, for all excitatory neurons. For the inhibitory neurons, this is multiplied by a constant $-g$, giving all the inhibitory neurons a PSP of amplitude $-gJ$. The connection probabilities between neurons are set to 0.1, meaning each neuron receives 1000 random excitatory and 250 random inhibitory connections.

The parameters that are fixed for the majority of simulations are given in table 3.2.

Table 3.2: Simulation parameters.

Parameter	Value
N_E	10000 Neurons
N_I	2500 Neurons
ϵ	0.1
C_E	1000 Connections
C_I	250 Connections
τ_m	20 ms
C_m	250 pF
V_m	0 mV
V_r	0 mV
θ	20 mV
E_L	20 mV
g	-5
J_E	0.15 mV
J_I	-0.75 mV
T	10 s
dT	0.1 ms
$Delay$	1.5 ms

To record the activity of both the excitatory and inhibitory neuron populations, spike recorders are connected to 50 randomly chosen excitatory neurons

and 50 randomly chosen inhibitory neurons. All simulations in this work were run using 10 different random seeds, and in all simulations were optimized using ProcessPoolExecutor from the concurrent.futures library (Python Software Foundation, 2023). This class allows us to run computations in parallel. One compute node at JUSUF consist of 128 CPUs, table 3.1. We divided the CPUs into 32 individual workers, each consisting of 4 CPUs. Each worker will run one simulation, allowing us to run 32 simulations in parallel.

3.3 Evaluation

The output from NEST is processed by the Neo library (Garcia et al., 2014) which creates SpikeTrain objects, where the firing rate is reported in spikes per millisecond. The Elephant library (Yegenoglu et al., 2018) is used for the statistical analysis, producing FR, CV, and CC. Calculating Wasserstein distances between 1-dimesional vectors appear to be straightforward, and several libraries are able to this calculation (Scipy, 2023), (POT, 2021). However, there does not appear to be any library that is able to calculate Wasserstein distances between multidimensional arrays. One procedure to calculate the Wasserstein distances has been proposed using the methods found in the Python Optimal Transport library (POT, 2021). First one has to calculate the cost matrix between the arrays using the dist()-method, available in this library. For two $(m{\times}n)$ arrays, this method returns a matrix $\mathbf{M}$, with dimensions $(m{\times}m)$. In this method we have to specify what distance metric we will use to compute the distances. Here we use Euclidian distances. The second step is to calculate the Wasserstein distances using the emd2()-method, based the calculated cost matrix. This method solves the earth movers distance problem and returns the cost of transportation using the following steps:

$$\min_{\gamma} = \langle \gamma, \mathbf{M} \rangle \tag{3.6}$$

$$s.t. \, \gamma \mathbf{1} = \mathbf{a} \tag{3.7}$$

$$\gamma^T \mathbf{1} = \mathbf{b} \tag{3.8}$$

$$\gamma \geq 0 \tag{3.9}$$

where $\mathbf{a}$ and $\mathbf{b}$ are the input vectors. The computation for the cost of

transport is given the following priority: **a**, then **b**, and finally **M** if no input vectors are provided, allowing us to calculate the cost of transport when no input vectors are provided.

3.4 Validation against Brunel

To ensure that we have results comparable to Brunel, the first simulation carried out was done to replicate figure 8 in Brunel (2000). To produce this figure, Brunel modelled the SR, SI fast, SI slow and AI regime. The parameter settings for these simulations are found in figure 7 in Brunel (2000), and the parameters for the different regimes are given in table 3.3. Note that this simulation is the only simulation where the reset potential, V_{reset}, is set to 10 mV. In all other simulations the reset potential is set to 0 ms. The main reason for setting the reset potential to 0 ms it that this is the default setting found in the NEST documentation, and that the dynamics of the alpha synapse was very difficult to control when reset potential was set to 10 ms. But in order to successfully replicate figure 8, the reset potential had to be set to 10 ms for this simulation. In Brunel's work, the Dirac delta function was used to model the synapse. In our experience it is easier to control the dynamics for the delta function, compared to the alpha function, when the reset potential was set to 10 ms, posing no problems for this set simulations. The parameters used to create the regimes in these simulations are given in table 3.3.

Table 3.3: Parameters for Brunel's figure 8.

Regime	V_{reset}	$Delay$	g	η
SR	10.0	1.5	3.0	2.0
SI fast	10.0	1.5	6.0	4.0
AI	10.0	1.5	5.0	2.0
SI slow	10.0	1.5	4.5	0.9

3.5   Parameter settings

The second set of simulations carried out was carried out to inspect the behavior of the different synapse models in the different regimes reported by Brunel. To define which regime a simulation is carried out in, the following parameters will be varied: delay, g, and η. These values are based on the values reported in figure 2 in Brunel (2000). The values for the SR, AI, SI fast and SI slow regimes are from figure 2 A and the values for the AR regime are form figure 2 C. The parameters for the different regimes are given in table 3.4. These parameter values produce the different regimes when the delta synapse is used. The simulations carried out using the other synapse models were run with the same set of parameters, but we cannot with certainty say that these models operate in the same regimes as the delta function.

Table 3.4: Parameters for the different regimes.

Regime	Delay	g	η
SR	1.5	2.0	2.0
AI	1.5	6.0	2.0
SI fast	1.5	7.0	3.5
SI slow	1.5	7.0	0.9
AR	2.0	2.0	2.0

The third set of simulations carried out was done to explore whether we could get the alpha and the single exponential decay synapse models models to display the same dynamics as the delta synapse in the different regimes. The following parameters were tuned τ_{syn}, τ_{mem}, and θ. The range in which each parameter were tuned generally was as follows: $\tau_{syn} = [0.5, 2.0]$ ms, $\tau_{mem} = [4.0, 40.0]$ ms, and $\theta = [10.0, 30.0]$ mV. However, some wider parameter ranges were explored using the alpha synapse in an attempt to get it's firing activity closer to the firing activity observed using the delta synapse. These values include parameters in the ranges of $\tau_{syn} = [0.1, 19.9]$ ms, $\tau_{mem} = [0.1, 1000.0]$ ms, and $\theta = [0.01, 40.0]$ mV.

The dynamics of a simulation was observed to change with small changes in parameters, within the borders of a regime. To further explore this, we

performed a set of simulations over small areas that cover each regime in figure 2 in Brunel (2000). The areas were explored by varying the inhibitory PSP multiplication factor, g, in an interval of length 1, with a resolution of 0.050. The external rate relative to the threshold rate, η, was varied in an interval of length 0.5, with a resolution of 0.025. The values g and η take on for each regime are given in table 3.5. The sweeping over the different areas was carried out for all three synapse models. In addition to sweeping over the selected areas in figure 2, we also performed a complete sweep over figure 2 A in Brunel. This was done on g-values between 0 and 8, with a resolution of 0.250, and η-values in the range 0 to 4, with a resolution of 0.125.

Table 3.5: Brunel regimes.

Regime	Delay	g	η
SR	1.5	1.0-2.0	1.5-2.0
AI	1.5	5.0-6.0	1.5-2.0
SI fast	2.0	7.0-8.0	3.0-3.5
SI slow	2.0	7.0-8.0	0.75-1.25
AR	2.0	2.0-3.0	1.5-2.0

Neural networks of different sizes have been reported to display different dynamics (Albada et al., 2015). To explore this effect, we run simulations for the three synapse models in networks of different sizes. We do this for all regimes, using the parameters given in table 3.4. The different network sizes explored were of order 250, 500, 1000, 2500 and 5000, resulting in networks consisting of 1250, 2500, 5000, 12500 and 25000 neurons, respectively. The connection probability is held constant, at $\epsilon = 0.1$, for all simulations, leading to a total of 25, 50, 100, 250 and 500 incoming synapses per neuron, respectively.

Chapter 4

Results

This chapter will present the results from the simulations. In the first section we present the raster plot from the simulation attempting to replicate figure 8 in Brunel (2000). Then we will present a section showing the results from running simulations using the different synapse models in the different regimes reported by Brunel, and show the different dynamics produced by each synapse model. This is followed by a section where we present the results from the simulations where we attempt to recreate the dynamics of the delta synapse using the alpha and the exponential decay synapse models. The next section will present the change in dynamics observed when simulations are run with different combinations of g and eta within the boundaries of each regime reported by Brunel. We will also display the dynamics observed when using different combinations of g and eta over the whole of figure 2 A in Brunel (2000), which include the AI, SR, and SI regimes, including both the fast and slow oscillation SI regime. These results are of lower resolution than the simulations run on individual regimes, but we will try to identify clear boundaries as displayed in the original figure. The results from all three synapse models will be displayed. The last section will present the results from varying the size of the network, and show the different dynamics observed when varying the size of the network for each of the three synapse models.

4.1 Replicating Brunel model dynamics

Raster plots provide information about the dynamics of a network, including a visual representation of the firing rate displayed by the neurons and the degree of synchronicity present in the network. We use raster plots to visually evaluate whether we are able to successfully replicate figure 8 in Brunel (2000). For the rest of this section, whenever we write figure 8, we refer to this figure from Brunel. The raw raster plots available in NEST resulting from these are shown in figure 4.1. These raster plots display the firing activity of 50 randomly selected excitatory neurons. In figure 4.1 b), c), and d), the activity of the network is displayed in a timeframe ranging from 800 ms to 1000 ms, while figure 8 B, C, and D in use a timeframe ranging from 1000 ms to 1200 ms. This is due to all our simulations being run for 1000 ms. We assume that the activity of the network stabilizes at around 200 ms, and that our timeframe will produce the same results as the results that simulating for another 200 ms would have produced.

Figure 4.1 a) shows the activity of the network in the SR regime. From the figure we observe that this regime is characterized by a high firing rate and a high degree of synchronicity. The firing rate displayed in the bottom part of figure 4.1 a) is close to 300 spikes per second on average. The dynamics in this figure is close to what is observed in figure 8 A. However, we do not observe the massive spikes observed in the firing rate in the bottom part of figure 8A. This is mainly due to the lower resolution of the plot provided by NEST. The average firing rate, represented by the dotted line, in figure 8 A is shown to be around 1/3 of the way between 0 and 1000, which is similar to our result, close to 300 spikes per second. The exact firing rate for this regime is not reported in Brunel (2000).

In figure 4.1 b), the raster plot showing the activity of the network in the fast oscillating SI regime is displayed. We observe that the firing rate is lower, around 60 spikes per second, and that the synchronicity of the firing is lower than observed in the SR regime. However, the synchronicity observed is higher than in the AR regime displayed in 4.1 c). The dynamics in 4.1 b) are similar to what as observed in figure 8 B and table 1 in Brunel (2000), where the firing rate is reported to be 60.7 spikes per second on average for this regime.
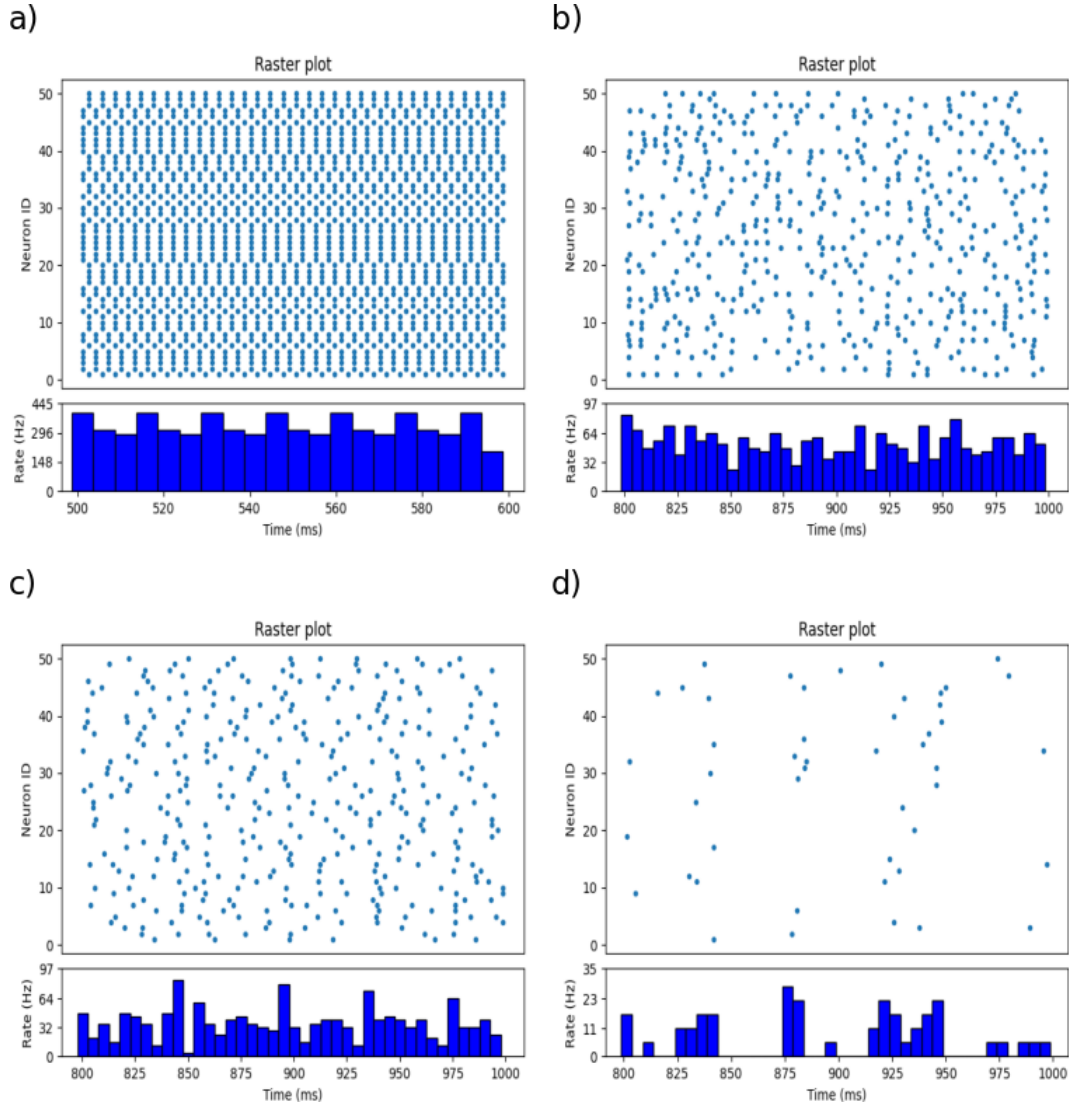
Figure 4.1: Raster plots from the reproduction of Brunel model dynamics. The raster plots show the firing of 50 randomly chosen excitatory neurons in the following regimes: a) synchronous regular, b) fast oscillating synchronous irregular, c) asynchronous irregular, and d) slow oscillating synchronous irregular regime.

Figure 4.1 c) shows the activity of the network in the AI regime. In this figure we observe that the firing rate is lower than in the fast oscillating SI regime and that there is very little synchronicity in the firing of the neurons. The firing rate appears to be around 30 spikes per second with some spikes where the activity is over 60 spikes per second. These dynamics are close to the dynamics observed in figure 8 C and table 1, where the firing is reported to be 37.7 spikes per second in this regime. The last subfigure, figure 4.1 d)

shows the activity of the network in the slow oscillating SI regime. The firing rate observed is very low, with some degree of synchronicity. For most of the time, the network is non-active, but we observe some spikes in activity. These dynamics are similar to what in observed in figure 8 D. When the activity is spiking, we observe a firing rate getting close to 30 spikes per second in the bottom part of figure 4.1 d). In Brunel (2000), the activity has higher spikes, with very short time duration. We do not observe this in figure 4.1 d), probably due to the wider time intervals in our plot. In table 1, the average firing rate for this regime is reported to be 5.5 spikes per second. This is close to what we observe in 4.1 d). The results shown in figure 4.1 are in accordance to figure 8. Since we are able to satisfactory replicate these results, we assume that the results produced for this thesis are comparable to the results reported by Brunel (2000).

4.2 The synapse models in the different regimes

This section will first present the results from the simulations done in the different regimes in a network consisting of 12500 neurons in detail. This is the same sized network as reported by Brunel (2000). The regimes we use are defined using the delta synapse and the parameters for the regimes are given in 3.4. For the alpha and exponential synapse models, we use the same set of parameters, and the results for the are presented as if these are in the same regime as the delta synapse model. The results presented include the following spiking statistics: the firing rate (FR) the coefficient of variation (CV) and the correlation coefficient (CC) and Wasserstein distances.

Figure 4.2 displays the empirical cumulative distribution function,(ecdf) for the FR, the CV and the CC. In table 4.1 the means and standard deviations of the FR, CV and CC for the different Brunel regimes are displayed. Table 4.2 present the Wasserstein distances between the simulations done in each regime, together with the within-regime Wasserstein distances. The results presented include results for all three synapse models, the delta, alpha and exponential decay synapse model.

In figure 4.2 the edcfs for the FR, CV and CC are shown. For each neuron, the mean spiking statistics are calculated across the ten differently seeded
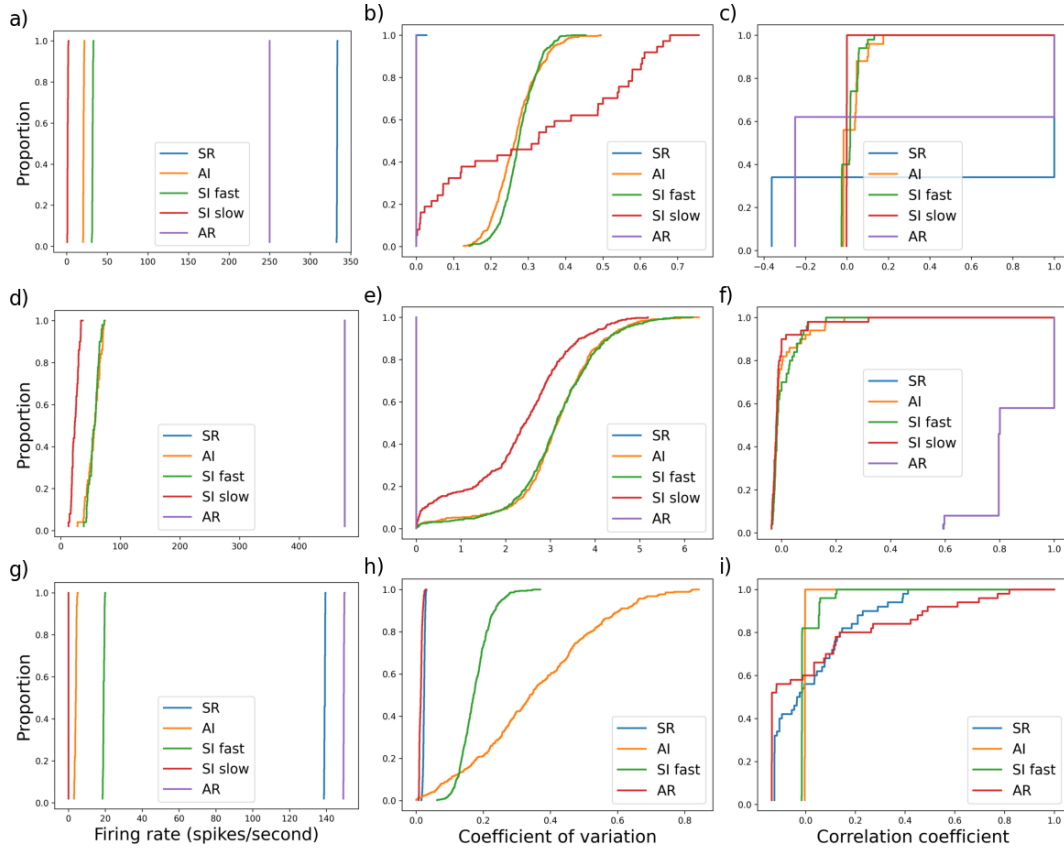
simulations. That is, for each of the 50 recorded neurons the spiking statistics are calculated for each of the differently seeded simulations. Then the mean is calculated for each neuron across these ten simulations. The results from the 50 neurons are plotted as an ecdf curve.

In table 4.1, the mean and standard deviations displayed for each regime are calculated across the 50 neurons in each simulation and across the 10 differently seeded simulation. In table 4.2, the within-regime Wasserstein distances are calculated from one seeded simulation in that regime to each of the other nine differently seeded simulations within that regime, separately. This is calculated for all the ten differently seeded simulations within that regime. Then the average and standard deviation are calculated across all these Wasserstein distances. The between Wasserstein distances are calculated from one seeded simulation in the first regime to all ten differently seeded in the second regime, separately. This is done for all ten different seeds in the first regime, then the average and standard deviation are calculated across all these Wasserstein distances.

Figure 4.2 a), d), and g) displays the FR ecdf curves for the delta, alpha and exponential decay synapse model, respectively. We observe that the range of the x-axis differs between the different synapse models, and that the maximum value for the FR differs between the different synapse models. We see that the x-axis for the alpha synapse model goes to 500 spikes per second, while it goes to 350 spikes per for the delta synapse and 150 spikes per second for the exponential decay synapse model. In all synapse models we see that the FR in the irregular regimes tend to group together, and that the FR is low compared to the regular regimes. For all synapse models, the regular regimes also tend to group together. In figure 4.2 a) we see that the distance between the FR in the AR and SR regimes is the largest for the delta synapse model, while in figure 4.2 d) the FR of the AR and SR regimes lie on top of each other for the alpha synapse, making it hard to distinguish between them.

For the CV ecdf curves, displayed in figure 4.2 b), e), and h), we observe that there is more variability in the irregular regimes than it is in the regular regimes. This is observed for all three synapse models. The regular regimes seem to have a CV very close to zero for all synapse models, so the individual neurons then to display the same activity for the duration of the simulation. However, we see that the range of the x-axis is almost 10 times as large for the

alpha synapse model, figure 4.2 e), as it is for the other synapse models. The reason being that the CV is very high for the alpha synapse in the irregular regimes. This may indicate that the alpha synapse model is in a different regime than the delta and exponential synapse model are for the parameter settings we used to define the irregular regimes.

Figure 4.2: Spiking statistics for the different synapse models in the different regimes. The firing rate (spikes/second), coefficient of variation and correlation coefficient are shown for the delta synapse model in a) - c), for the alpha synapse model in d) - f), and for the exponential decay synapse model in g) - i), respectively. The exponential decay synapse model does not have any neuron firing in the SI slow regime, and the SI slow regime is not included in h) and i). For each neuron, the mean spiking statistics are calculated across the ten differently seeded simulations. That is, for each of the 50 recorded neurons the spiking statistics are calculated for each of the differently seeded simulations. Then the mean is calculated for each neuron across these ten simulations and plotted as an empirical cumulative distribution function.

From the CC ecdf curves in figure 4.2 c), f), and i) we see that most of the neurons in the irregular regimes have a CC close to 0 for all three synapse models. For the regular regimes, the variability of the CC is a bit larger for the exponential decay synapse model, as we can see in 4.2 i). For the other

two synapse model the CC is larger for most of the neurons in the regular regimes. For the delta synapse model, we observe in figure 4.2 c) that the CC takes the largest values for the SR regime, in absolute value. For the alpha synapse model, figure 4.2 f), the CC is overlapping for the regular regimes and all neurons have a CC of roughly 0.6 and above.

From table 4.1, we observe that the regimes characterized by neurons with irregular firing activity have lower firing rates than the regimes characterized by neurons that fire more regularly. This observation is consistent across the three different synapse models. We also observe that the firing rates for the alpha synapse model is higher than for the other synapse models in all regimes. In both the regular regime the alpha synapse model displays an average firing rate of 476.25 spikes per second, with zero, or close to zero, standard deviation. In the irregular regimes however, the standard deviation observed in the firing rate is very high for the alpha synapse compared to the other models.

The exponential decay model shows the lowest firing rate of the three synapse models. This is consistent across all the different regimes. Note that in the slow oscillating synchronous irregular regime the firing rate is zero for this synapse model. The standard deviations we observe in the firing rates are lower in the irregular regimes compared to the other synapse models. However, the standard deviations of the firing rate in the regular regimes are higher for the exponential decay model than for the delta model.

For all three synapse models, the coefficient of variation reported in table 4.1 are lower in the regular regimes, compared to the regimes with irregular firing. For the alpha synapse, the coefficient of variation is zero in the regular regimes, meaning that the individual neurons fire with the same rate over time. In the other synapse models, the CVs in the regular regimes are also close to zero with close to zero standard deviation. This indicates that the firing of the individual neurons in these regimes is very consistent over time. In the irregular regimes, the CV observed for the delta and exponential models are of the same order. In the AI regime the CV is higher for the exponential synapse, while for the fast oscillating SI regime the delta synapse shows a higher CV. In both cases, we observe that if the CV is higher, the standard deviation will also be higher. Since there is no firing for the exponential decay model in the slow oscillating SI regime, the CV is 0. For the alpha synapse model, we observe CVs that are generally of an order of 10 higher to what is observed

for the other synapse models. The CVs for the alpha synapse also have higher
standard deviations compared to the other synapse models, meaning that in
these regimes the firing of the individual neurons in the networks using the
alpha synapse is less regular than in the networks using the other synapse
models. To us it appears that the alpha synapse model is operating in a
different regime for the parameter settings accompanied with the irregular
regimes when using the delta synapse model, given in 3.4.

The correlation coefficient displayed in table 4.1 show the same pattern in
all three synapse models. The CCs are high for the regular regimes and low for
the irregular regimes. In the regular regimes, the alpha synapse displays the
highest values with a CC of 0.836, meaning that the firing between the neurons
in the network is happening in a very synchronous fashion. This is consistent
with the observations from the firing rate and the CV and strengthens our
belief in that the firing has reach some type of ceiling, and that all the recorded
neurons are firing at this rate. For the exponential decay model, the observed
CC is low in the SR regime compared to the other models and the AR regime.
In the irregular regimes, all observed CCs are of the same order and have very
similar standard deviations of around 0.14. Except for the slow oscillating SI
for the exponential decay model where it is zero.

Table 4.1: Spiking statistics for each regime, using the a) delta synapse model, b) alpha synapse model, and c) exponential decay synapse model. In this table, the mean and standard deviations are calculated across the 10 differently seeded simulations and the 50 neurons in each simulation. The parameters in the different regimes are as follows: SR: $D = 1.5, g = 2.0, \eta = 2.0$, AI: $D = 1.5, g = 2.0, \eta = 2.0$, SI fast: $D = 1.5, g = 7.0, \eta = 3.5$, SI slow: $D = 1.5, g = 7.0, \eta = 0.9$, and AR: $D = 2.0, g = 2.0, \eta = 2.0$.

a) Delta synapse			
Regime	**FR (spikes/s)**	**CV**	**CC**
SR	333.06 ± 0.62	0.000 ± 0.001	0.266 ± 0.678
AI	20.85 ± 1.54	0.268 ± 0.061	0.027 ± 0.144
SI fast	32.02 ± 1.76	0.277 ± 0.047	0.028 ± 0.143
SI slow	1.32 ± 1.16	0.330 ± 0.244	0.017 ± 0.133
AR	250.00 ± 0.00	0.000 ± 0.000	0.338 ± 0.629
b) Alpha synapse			
Regime	**FR (spikes/s)**	**CV**	**CC**
SR	476.25 ± 0.00	0.000 ± 0.000	0.836 ± 0.156
AI	56.18 ± 33.46	3.119 ± 1.018	0.022 ± 0.151
SI fast	56.20 ± 34.09	3.124 ± 1.016	0.024 ± 0.151
SI slow	24.27 ± 19.88	2.289 ± 1.203	0.014 ± 0.133
AR	476.25 ± 0.07	0.00 ± 0.00	0.836 ± 0.156
c) Exponential decay synapse			
Regime	**FR (spikes/s)**	**CV**	**CC**
SR	139.07 ± 0.98	0.024 ± 0.003	0.051 ± 0.208
AI	3.96 ± 0.57	0.357 ± 0.187	0.019 ± 0.142
SI fast	19.18 ± 1.06	0.176 ± 0.046	0.022 ± 0.144
SI slow	0.00 ± 0.00	0.00 ± 0.00	0.00 ± 0.00
AR	149.45 ± 0.63	0.014 ± 0.004	0.151 ± 0.345

Table 4.2: Wasserstein distances between each regime, using the a) delta synapse model, b) alpha synapse model and c) exponential decay synapse models. In this table, the within-regime Wasserstein distances are calculated from one seeded simulation in that regime to each of the other nine differently seeded simulations within that regime, done separately. This is calculated for all the ten differently seeded simulations within that regime. Then the average and standard deviation are calculated across all these Wasserstein distances. The between Wasserstein distances are calculated from one seeded simulation in the first regime to all ten differently seeded in the second regime, done separately. This is done for all ten different seeds in the first regime, then the average and standard deviation are calculated across all these Wasserstein distances.

a) Delta synapse

Regime	AI	SI fast	SI slow	AR	SR
AI	2.1 ± 1.2	14.0 ± 8.0	23.8 ± 13.6	270.8 ± 154.8	366.2 ± 209.4
SI fast	14.0 ± 8.0	2.9 ± 1.7	37.4 ± 21.4	257.2 ± 147.0	352.6 ± 201.6
SI slow	23.8 ± 13.6	37.4 ± 21.4	1.7 ± 1.0	294.4 ± 168.3	389.8 ± 222.8
AR	270.8 ± 154.8	257.2 ± 147.0	294.4 ± 168.3	0.9 ± 0.5	95.7 ± 54.7
SR	366.3 ± 209.3	352.6 ± 201.5	389.8 ± 222.8	95.7 ± 54.7	0.97 ± 0.5

b) Alpha synapse

Regime	AI	SI fast	SI slow	AR	SR
AI	45.5 ± 26.0	50.0 ± 28.7	56.6 ± 32.1	502.7 ± 287.7	503.9 ± 288.3
SI fast	50.6 ± 28.5	47.1 ± 26.86	58.0 ± 32.9	503.3 ± 286.3	503.4 ± 287.6
SI slow	56.3 ± 32.5	57.46 ± 33.1	27.7 ± 15.8	538.9 ± 308.5	540.1 ± 309.1
AR	502.8 ± 287.4	502.3 ± 287.1	502.8 ± 308.1	0.5 ± 0.3	1.3 ± 0.7
SR	503.9 ± 288.1	503.4 ± 287.7	540.1 ± 308.7	1.3 ± 0.7	0.1 ± 0.1

c) Exponential decay synapse

Regime	AI	SI fast	SI slow	AR	SR
AI	0.0 ± 0.0	3.4 ± 0.6	1.1 ± 0.2	30.9 ± 5.3	28.9 ± 4.9
SI fast	1.9 ± 1.0	1.4 ± 0.8	22.9 ± 13.1	145.5 ± 83.2	135.2 ± 77.3
SI slow	0.7 ± 0.3	22.8 ± 13.1	0.0 ± 0.0	168.2 ± 96.2	157.8 ± 90.2
AR	17.8 ± 9.3	145.5 ± 83.2	168.2 ± 96.2	0.9 ± 0.5	10.5 ± 6.0
SR	16.7 ± 8.7	135.4 ± 77.3	157.9 ± 90.1	10.4 ± 6.1	1.3 ± 0.7

4.3   Recreating the dynamics of the delta synapse

The results of our attempt to recreate the dynamics of the delta synapse model using the alpha and exponential decay synapse model is displayed in table 4.4. In this table we try to make the alpha and exponential decay synapse models display similar spiking statistics as shown for the delta synapse model in table 4.1. The parameters combinations that made the dynamics as close to the delta synapse model are displayed in table 4.3.

In general, making the exponential decay synapse model behave as the delta synapse model required less effort, and required searching over a smaller parameter space than was required for the alpha synapse model. This was the case for all regimes. In table 4.4 we see that we were not able to dampen the firing activity of the alpha synapse model in the regular regimes. By setting extreme parameter values, we were able to reduce the firing rate by a couple of spikes per second for the alpha synapse model in this regime. This is very far away from the dynamics of the delta synapse in these regimes, and it appears do be very difficult to reduce the firing rate of the alpha synapse model in the regular regimes. In the irregular regimes we were able to make the firing rate and CC of the alpha synapse close those observed by the delta model. However, the CV is generally an order of 10 higher for the alpha synapse model than for the delta model. For the exponential decay synapse model, we were able to get close the dynamics of the delta synapse in all regimes, and we were able to get all three spiking statistics close to those displayed by the delta synapse model.

Table 4.3: The parameter settings that made the alpha and the exponential decay synapse model display dynamics similar to that of the delta synapse model.

a) Alpha synapse			
Regime	τ_{syn}	τ_{mem}	θ
SR	10.0	20.00	0.5
AI	0.5	25.0	0.2
SI fast	1.0	20.0	10.0
SI slow	1.0	5.0	0.01
AR	18	20	0.5
b) Exponential decay synapse			
Regime	τ_{syn}	τ_{mem}	θ
SR	2.0	17.5	20.0
AI	0.7	17	15
SI fast	1.0	15.0	15.0
SI slow	1.0	15.0	17.5
AR	0.7	20.0	20.0

Table 4.4: Spiking statistics from making the alpha- and exponential decay synapse model show the same dynamics as the delta synapse model. a) Spiking statistics from the delta synapse model included for reference. b) Spiking statistics for the alpha synapse model. c) Spiking statistics for the exponential synapse model.

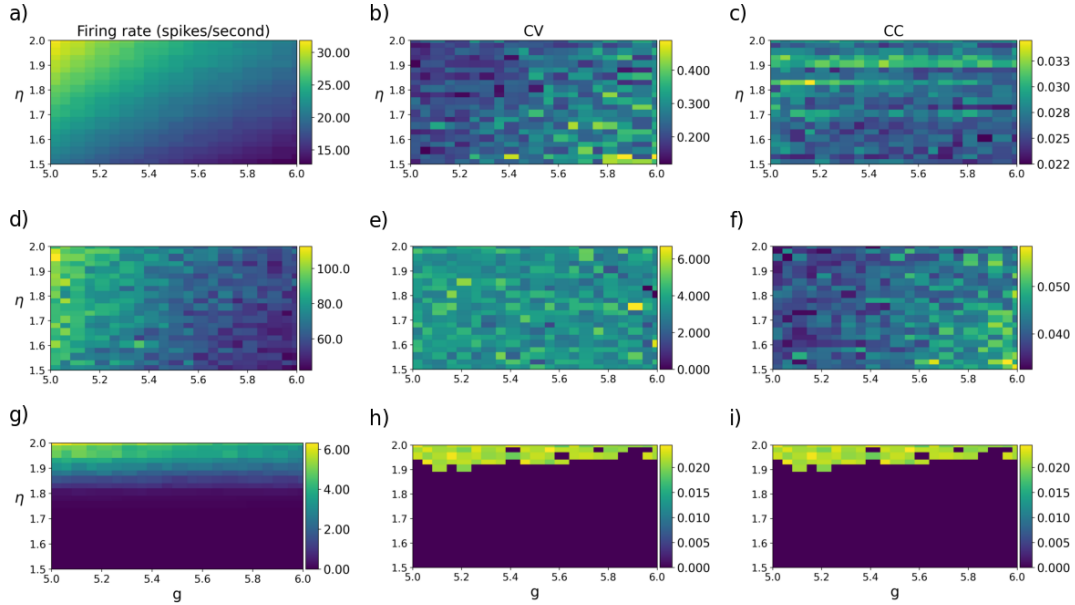| a) Delta synapse			
Regime	**FR (spikes/s)**	**CV**	**CC**
SR	333.06 ± 0.62	0.000 ± 0.001	0.266 ± 0.678
AI	20.85 ± 1.54	0.268 ± 0.061	0.027 ± 0.144
SI fast	32.02 ± 1.76	0.277 ± 0.047	0.028 ± 0.143
SI slow	1.32 ± 1.16	0.330 ± 0.244	0.017 ± 0.133
AR	250.00 ± 0.00	0.000 ± 0.000	0.338 ± 0.629
b) Alpha synapse			
Regime	**FR (spikes/s)**	**CV**	**CC**
SR	474.31 ± 0.47	0.00 ± 0.00	0.40 ± 0.54
AI	19.98 ± 16.17	2.8 ± 1.31	0.03 ± 0.160
SI fast	32.50 ± 21.59	2.78 ± 0.78	0.06 ± 0.15
SI slow	1.00 ± 5.40	1.46 ± 1.76	0.03 ± 0.18
AR	472.90 ± 0.42	0.00 ± 0.00	0.10 ± 0.56
c) Exponential decay synapse			
Regime	**FR (spikes/s)**	**CV**	**CC**
SR	329.42 ± 0.65	0.01 ± 0.59	0.06 ± 0.25
AI	20.44 ± 1.18	0.26 ± 0.06	0.03 ± 0.14
SI fast	33.39 ± 1.99	0.34 ± 0.05	0.05 ± 0.14
SI slow	1.32 ± 1.09	0.45 ± 0.20	0.02 ± 0.13
AR	246.85 ± 0.74	0.02 ± 0.00	0.02 ± 0.21

4.4 Sweeping over regimes

Figure 4.4 to figure 4.8 display the heatmaps produced when sweeping over the regimes presented in Brunel (2000). In order, each figure shows the dynamics of the following regimes: the asynchronous irregular, the fast oscillating synchronous irregular, the slow oscillating synchronous, the asynchronous regular and the synchronous regular regime. The individual subplots in each figure display the different spiking statistics calculated during each parameter sweep, including the firing rate, the coefficient of variation and the correlation coefficient. The intensity plotted in each heatmap represents the value of the respective spiking statistic in that subplot. As reference, we have made a sketch of figure 2 A and C from Brunel (2000). This is displayed in figure 4.3, where the parameter sweeps we have performed are marked by the red areas.
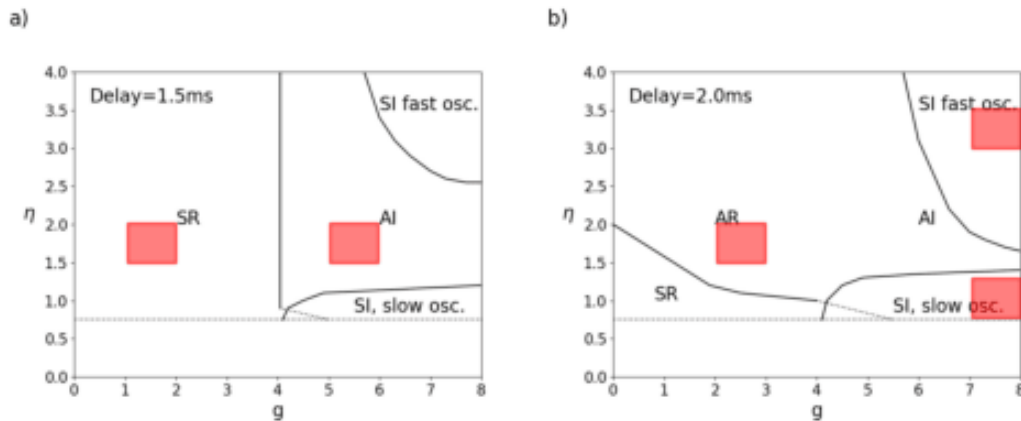
Figure 4.3: Sketch of the regimes identified by Brunel. In a) the delay is set to 1.5 ms, giving us access to the AI and SR regimes, and in b) the delay is set to 2.0 ms, giving us access to the AR regime and larger areas for the SI regimes. The red boxes indicate the areas where we sweep over the different values of g and η.

In figure 4.4 – figure 4.6 the spiking statistic for the irregular regimes are shown. We see that the spiking statistics varies within all regimes for all synapse models, except for the exponential decay model in the SI slow regime, where there is no firing for this synapse model in whole area explored. In all irregular regimes, the alpha synapse model is displaying the most variability in spiking dynamics and the exponential decay synapse model is displaying the least variability, and variability displayed by the delta synapse model lies in between.
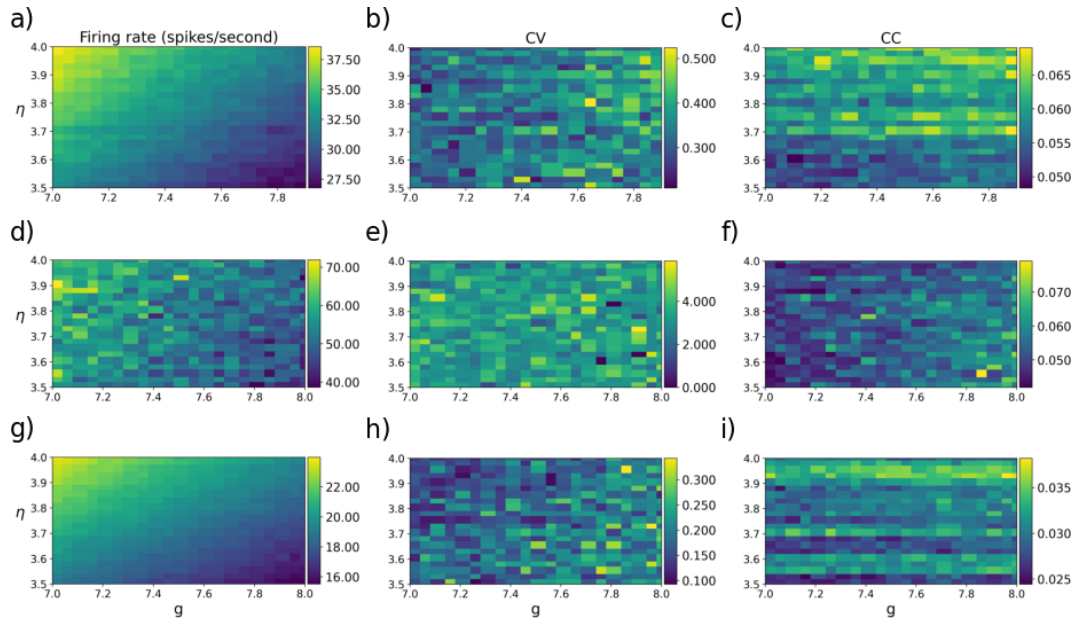
Figure 4.4: Brunel area sweep, AI regime. The firing rate (spikes/second), coefficient of variation and correlation coefficient are shown for the delta synapse model in a) - c), for the alpha synapse model in d) - f), and for the exponential decay synapse model in g) - i), respectively.

In the AI regime, we see that the firing rate and CV more than doubles its value within the regime for all three synapse models, while there is less variability observed in the CC. It is worth noting than a large part of this regime displays no firing activity for the exponential decay synapse model, making it hard to separate between these parts and the slow oscillating SI regime.

The variability observed in spiking statistics in the fast SI regime is generally smaller than what is observed in the AI regime, but there are some overlapping values between these two regimes for the alpha synapse model. For the delta synapse model, the firing rate and CV is generally a bit higher in the fast SI regime than in the AI regime, but there are some clear overlapping values for this synapse model as well. The CC displays similar variability as in the AI regime, making it hard to separate between the two regimes for the alpha and delta synapse models. The exponential decay synapse model has firing in the whole area of this regime and display a firing rate that is higher than in the active parts AI regime, making it possible to separate between these regimes for the exponential decay synapse model.
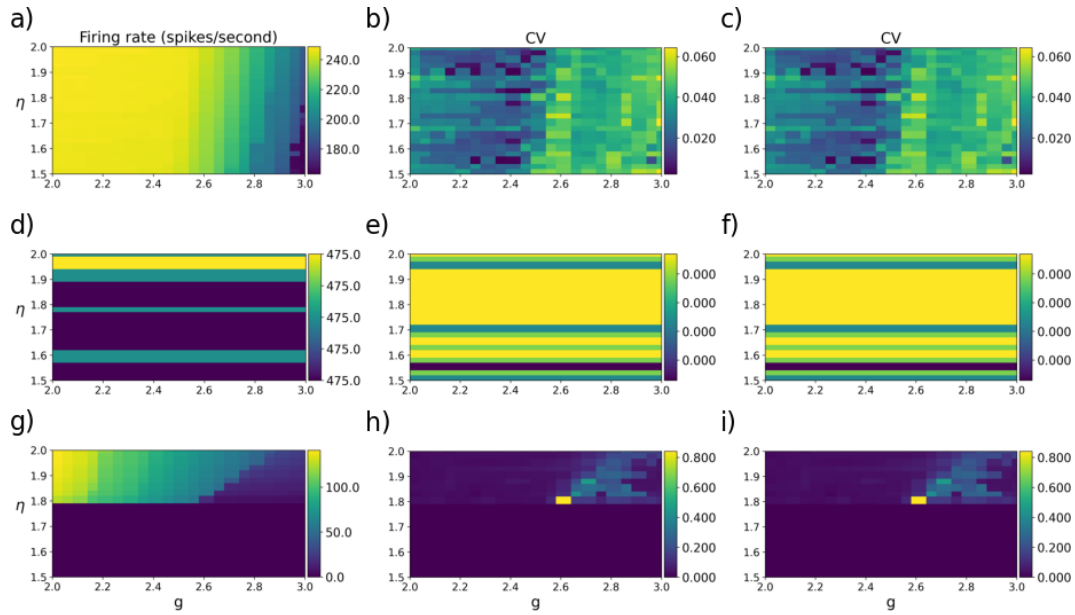
Figure 4.5: Brunel regime sweep, SI fast. The firing rate (spikes/second), coefficient of variation and correlation coefficient are shown for the delta synapse model in a) - c), for the alpha synapse model in d) - f), and for the exponential decay synapse model in g) - i), respectively.
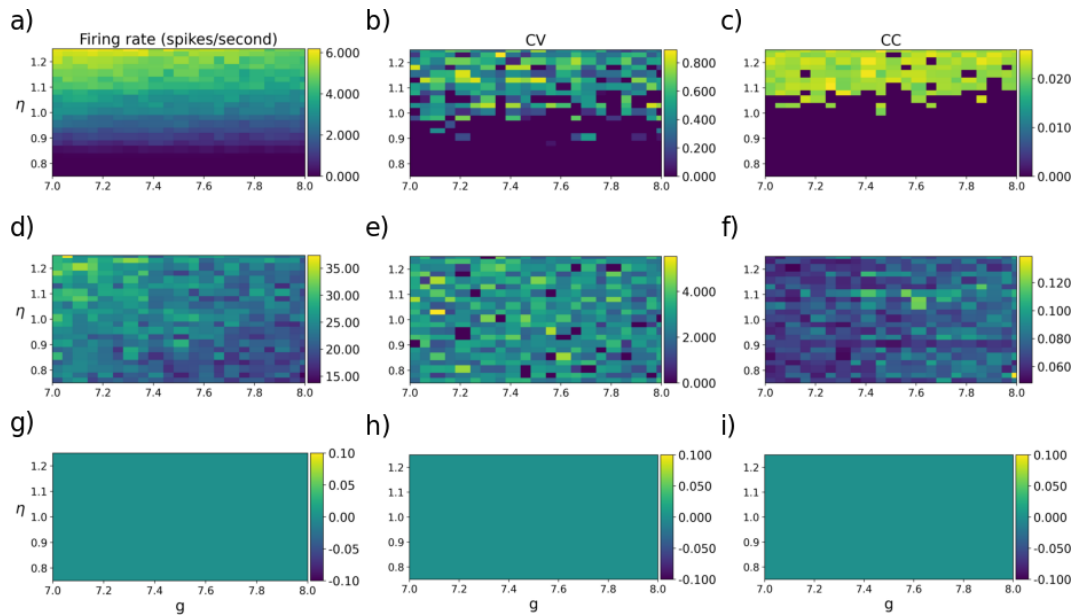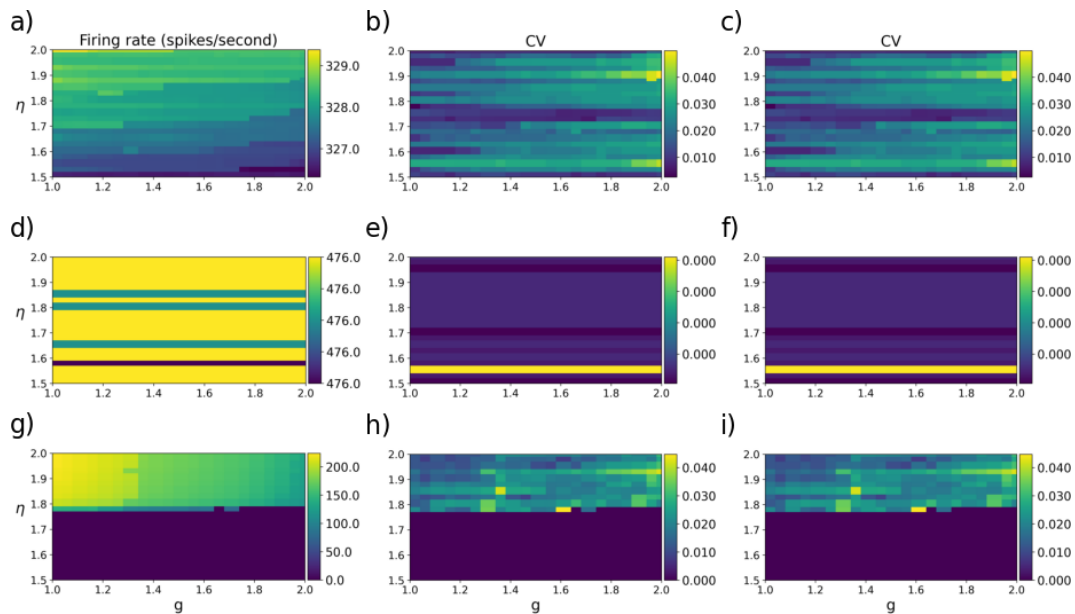

Figure 4.6: Brunel regime sweep, SI slow. The firing rate (spikes/second), coefficient of variation and correlation coefficient are shown for the delta synapse model in a) - c), for the alpha synapse model in d) - f), and for the exponential decay synapse model in g) - i), respectively.

In both of the regular regimes, figure 4.7 – figure 4.8, the alpha synapse model is displaying quite uniform dynamics in all of the selected areas. This includes a very high firing rate, a very low CV and very low CC, making it impossible to distinguish between the two regimes. However, the differences between the regular and irregular regimes are clear. In both regimes, we observe that the exponential decay synapse model does not fire in parts of the area. This happens for η values lower than roughly 1.8. The CV and CC for this synapse model is generally low in both regimes, but in the AR regime the firing rate tend to be in the range between 50 and 100 spikes per second, and in the SR regime the firing rate tend to be in the range between 100 and 200 spikes per second, making it possible to separate between the regimes on the firing rate. It is worth noting that in both regimes, there is a lot of variability in the firing rate within the regimes, and there is one point in the selected area of the AR regime that has a very high CV and CC. This makes it more difficult to draw up clear boundaries between the regimes. For the delta synapse model, the CV and CC are very similar in both regimes, but the firing rate is over 320 spikes per second in the SR regime, while it is lower than 230 spikes per second in the AR regime. We also see that the variability of the firing rate is higher in the AR regime than in the SR regime, making it possible to clearly distinguish between these two regimes based on the firing rate. For both the delta and exponential decay synapse model the separation between the regular and irregular regimes is clear.

Figure 4.7: Brunel regime sweep, AR regime. The firing rate (spikes/second), coefficient of variation and correlation coefficient are shown for the delta synapse model in a) - c), for the alpha synapse model in d) - f), and for the exponential decay synapse model in g) - i), respectively.

Figure 4.8: Brunel regime sweep, SR regime. The firing rate (spikes/second), coefficient of variation and correlation coefficient are shown for the delta synapse model in a) - c), for the alpha synapse model in d) - f), and for the exponential decay synapse model in g) - i), respectively.

In figure 4.9 to figure 4.11 we show the heatmaps produced from sweeping over the complete area of figure 2 A in Brunel (2000). Each figure includes parameter combinations that, when using the delta model, produce the AI, the fast oscillating SI, the slow oscillating SI and the SR regimes. Figure 4.9 shows the dynamics produced by the delta synapse model, figure 4.10 shows the dynamics produced by the alpha model, and 4.11 show the dynamic produced by the exponential decay model. The subplots in each figure show heatmaps displaying the calculated firing rate, coefficient of variation and correlation coefficient calculated from the respective synapse model. The intensity of each heatmap has been modified by the PowerNorm method available in the Matplotlib library (Matplotlib, 2021), with a gamma set to 0.1. This is done to give less of the available color scale to the regular regimes, and more of the available color scale to the irregular regimes. The point of this is to try to make the possible differences present between the irregular regimes more visible.
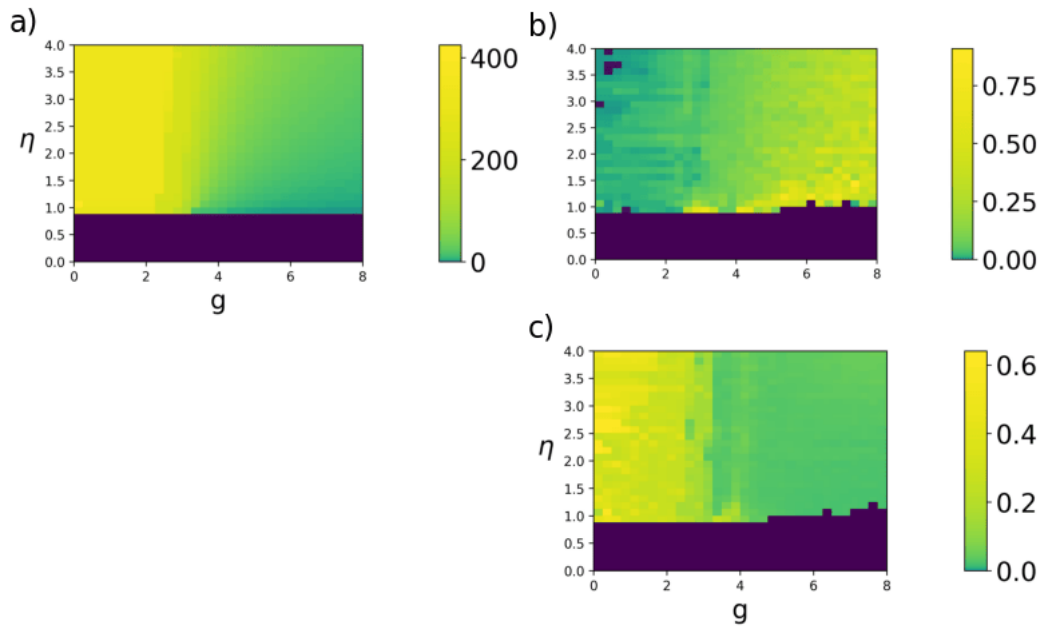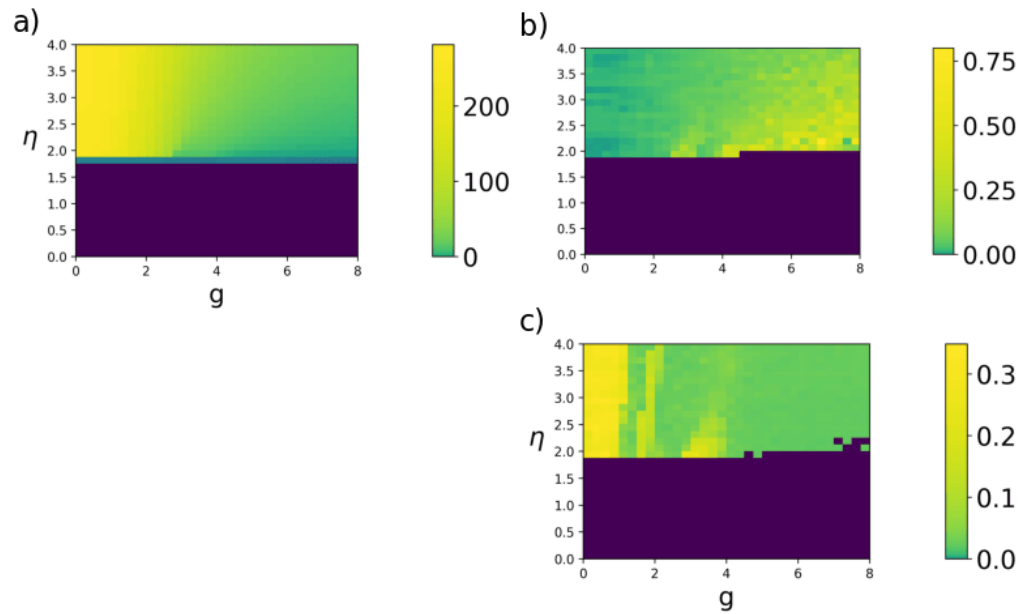

Figure 4.9: Full graph sweep, delta synapse. a) Firing rate (spikes/second), b) Coefficient of variation, c) Correlation coefficient.

The separation between the SR regime and the irregular regimes is very clear in figure 4.9 – figure 4.11 when looking at the firing rate and CV for all three synapse models. For the delta and alpha synapse models the separation is also very clear using the CC. However, for the exponential decay synapse model the CC tend to vary a bit in the SR regime, and at some points it takes on values that are generally found in the irregular regimes. When we look at the irregular regimes, the separation between the regimes does not appear to be very clear. For the delta model, we observe some differences in parts of the slow oscillating SI regime and the AI regime. The the main difference is that the CV and CC drops to zero in the parts of the slow oscillating SI regime with the lowest η- and highest g-values. For the AI and the fast oscillating SI it is difficult to find any pattern that would lead us to believe that there are any lines of clear separation between these regimes. For the delta synapse model there does not seem to be any pattern in any of the spiking statistics suggesting that there exist some clear lines of separation between the irregular regimes. The exponential decay synapse model does not have any neuron firing in the slow oscillating SI regime, however there is no neuron firing in the proximities of this regime and the line separating this regime does not exist for the exponential synapse model. For the AI regime, there are parts of the area that does not have any neuron firing. There does not appear to be any clear changes in any of the spiking statistics moving from the AI regime to the fast oscillating SI regime.

It is worth noting that we observe that for the delta synapse, the neuron firing stops at η-values at roughly 0.9 and below. In Brunel (2000), this stop in neuron firing was reported to theoretically happen at η-values of roughly 0.75 and below. For the exponential decay synapse model, the stop in firing happens at η-values of roughly 1.75 and below, whereas for the alpha synapse model the stop in neuron firing seem to only stop at η-values of 0.1 and below.
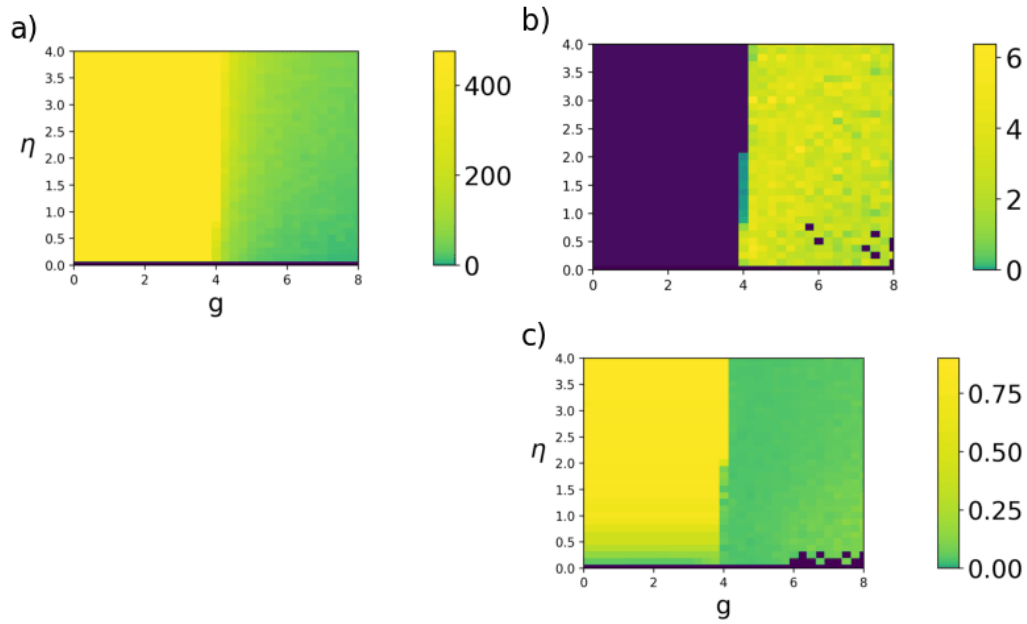
Figure 4.10: Full graph sweep, alpha synapse. a) Firing rate (spikes/second), b) Coefficient of variation, c) Correlation coefficient.


Figure 4.11: Full graph sweep, exponential decay synapse. a) Firing rate (spikes/second), b) Coefficient of variation, c) Correlation coefficient.

4.5   Effect of network size

In presenting the sizes of the networks, the sizes are referred to as order. When building the networks, the number of excitatory neurons in the network is four times the order and the number of inhibitory is one times the order. This means that the size of the smallest network, with order 250, is $4 \cdot 250 + 250 = 1250$ neurons.

The spiking statistics produced by the different the sized networks, in the different regimes, are displayed as horizontal bars in figure 4.12, 4.13, and 4.14 for the delta, alpha and exponential synapse models, respectively. In addition, the Wasserstein distances between the different regimes within each of the different sized network are displayed in figures 4.15 - 4.17. For all three synapse models the network sizes displayed are of order 250, 500, 1000, 2500, and 5000. Note that a network of order 2500 is of the same size as the network used in all other simulations, and the results in the section are close to what is reported in the synapse models in the different regimes section.
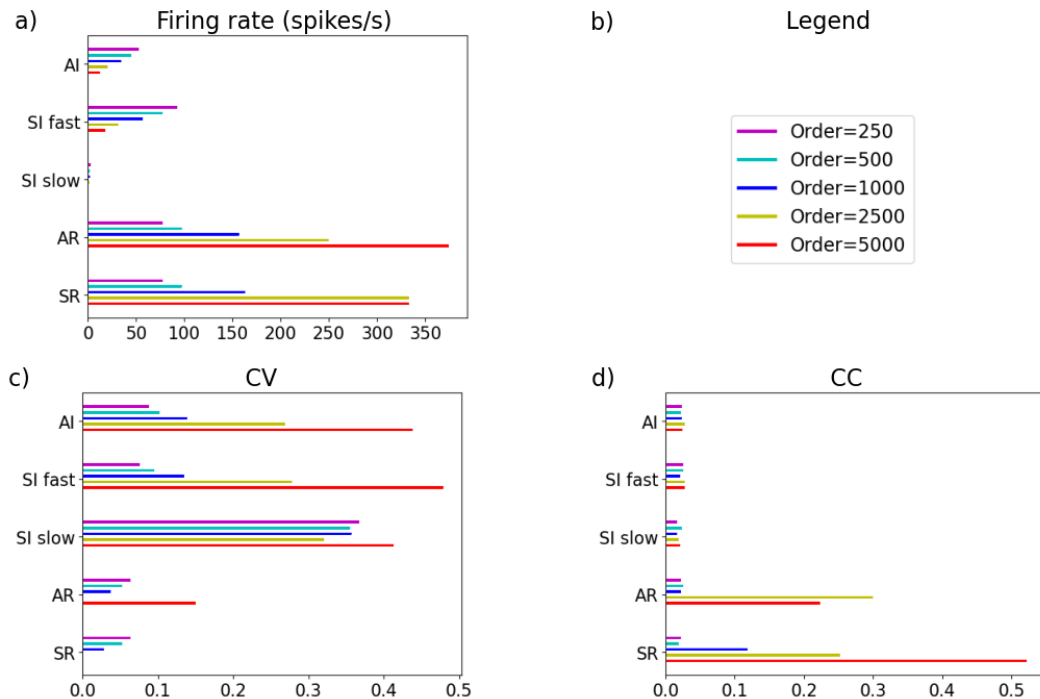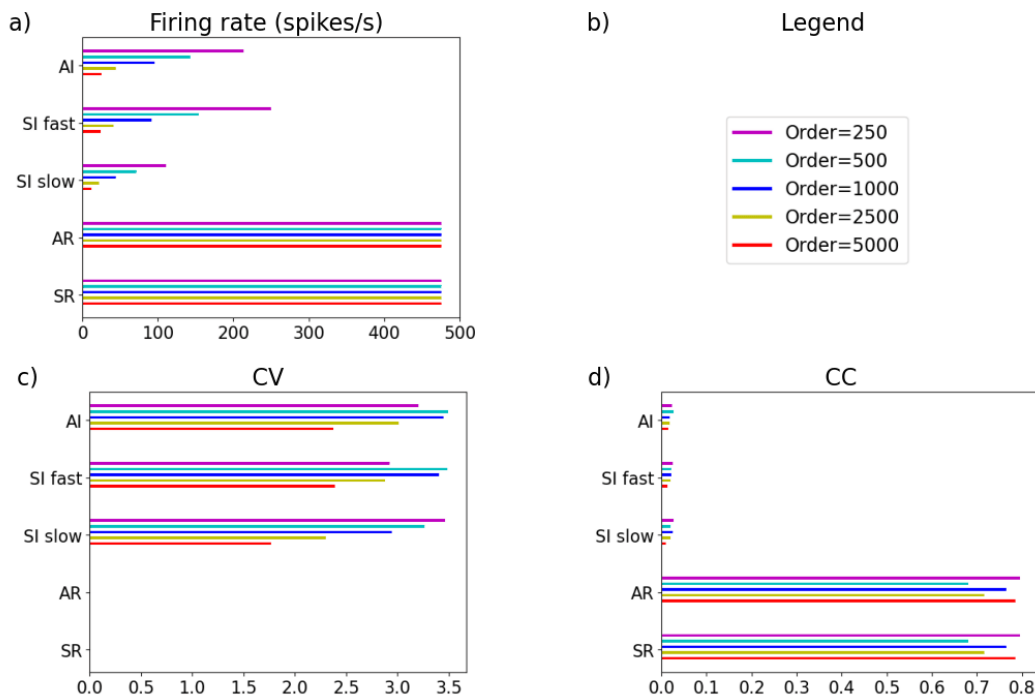

Figure 4.12: Spiking statistics for the delta synapse model in networks of different sizes. The spiking statistics displayed include: a) firing rate (spikes/second), c) coefficient of variation, d) correlation coefficient.

In figure 4.12 to figure 4.14 we see that the three different synapse models follow the same trend when the size of the network is increased. In the irregular regimes we see that as the size of the network is increases, the firing rates in the network decrease. This is true for all three synapse models, except for the exponential decay model in the slow oscillating synchronous irregular regime, where there is no neuron firing for all network sizes. The fall in firing rate is accompanied with an increase in CV when the network size is increased. All simulations in the irregular regimes where firing is observed, the CV is increasing as the size of the network is increased, except for the slow oscillating synchronous regime with the delta model. In this regime, we observe an increase in CV when the size of the network is increased from an order of 2500 to 5000. The CC in the irregular regimes display little variation between the different network sizes, compared to the firing rate and CV. In the delta synapse model, there seem to be a small increasing trend in CC as the size of the network is increasing. For the exponential synapse model, the trend seems to be a falling CC in the asynchronous regime, and the trend seem to be an increasing CC for the fast oscillating synchronous irregular regime as the size of the network is increasing. In the slow oscillating synchronous regime, the CC is zero due to no neural firing. The trends observed in the alpha and exponential synapse models are very small and may just be a result of random variation. For the delta synapse model, a stronger trend present, compared to the other two synapse models. Here the CC decrease as the size of the network is increasing, and this trend does not appear to be a result of randomness.

In the regular high firing regimes, the trend is different from the irregular regimes. For the delta and exponential decay model, the firing rate is strictly increasing as the size of the network is increasing, except for the delta synapse in the synchronous regular regime. In this regime the firing rate is the same for network sizes of 2500 and 5000. The typical trend of a falling CV as the firing rate is increasing is observed for both of these synapse models in the regular regimes, where the CV is strictly falling as the size on the network is increasing. The CV gets very close to zero as the network size increase to 2500 for the delta synapse model and as the network increase to 5000 for the exponential decay synapse model. There is one clear exception to this trend. As the network increase in size from 2500 to 5000, the CV is increasing for the alpha synapse in the asynchronous regime. The CC is generally increasing as

the size of the network is increasing in these regimes for both the alpha and exponential decay synapse models. There are two notable exceptions to this trend. In the exponential decay synapse model, there is a drop in the CC as the networks reach a size of 2500 in both regimes. In addition, there is a large spike in the CC observed for the delta synapse in the asynchronous regime when the network size is 2500. It is noteworthy that the observations for the delta synapse in the asynchronous regime, with a network size of 2500, appears to display some dynamics not persistent with the general trends observed in this regime for the other sized networks. Especially as it is common to use this synapse model and this network size for modelling, and is used in the work by (Brunel, 2000).


Figure 4.13: Spiking statistics for the alpha synapse model in networks of different sizes. The spiking statistics displayed include: a) firing rate (spikes/second), c) coefficient of variation, d) correlation coefficient.
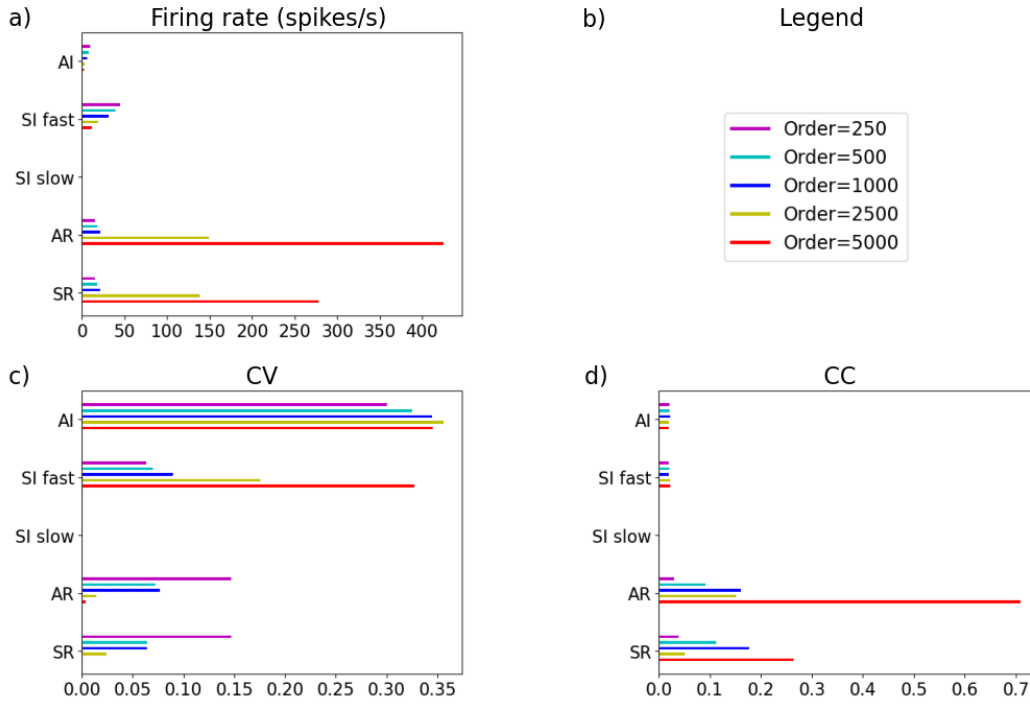
Figure 4.14: Spiking statistics for the exponential decay synapse model in networks of different sizes. The spiking statistics displayed include: a) firing rate (spikes/second), c) coefficient of variation, d) correlation coefficient.

Heatmaps displaying the Wasserstein distances between the different regimes using the delta synapse model in the different network sizes are showed in figure 4.15. For all network sizes, and all regimes, the within-regime Wasserstein distances are small. We also see that the two regular regimes tend to have small Wasserstein distances between each other. However, as the network size increase to an order of 2500 and above we start to see some separation between these regimes. In the irregular regimes, we see the same pattern in Wasserstein distances repeating itself for all network sizes. However, when the network size is small, the Wasserstein distances between the irregular regimes are relatively large compared to in the networks of size 1000 and larger. Interestingly, we observe that for order 250 the largest Wasserstein distance observed is between the asynchronous irregular regime and the fast oscillating synchronous irregular regime, and not between an irregular and a regular regime. In all other network sizes the largest distances observed are between an irregular and regular regime. These Wasserstein distances are largest between the asynchronous irregular regime and the regular regimes, but it varies which regular regime is the furthest away from the asynchronous regime. The general trend we observe when increasing the network size is that the separation between the regular and irregular regimes clearer, as the Wasserstein distances between these two groups increase a lot compared to the within-group Wasserstein distances.
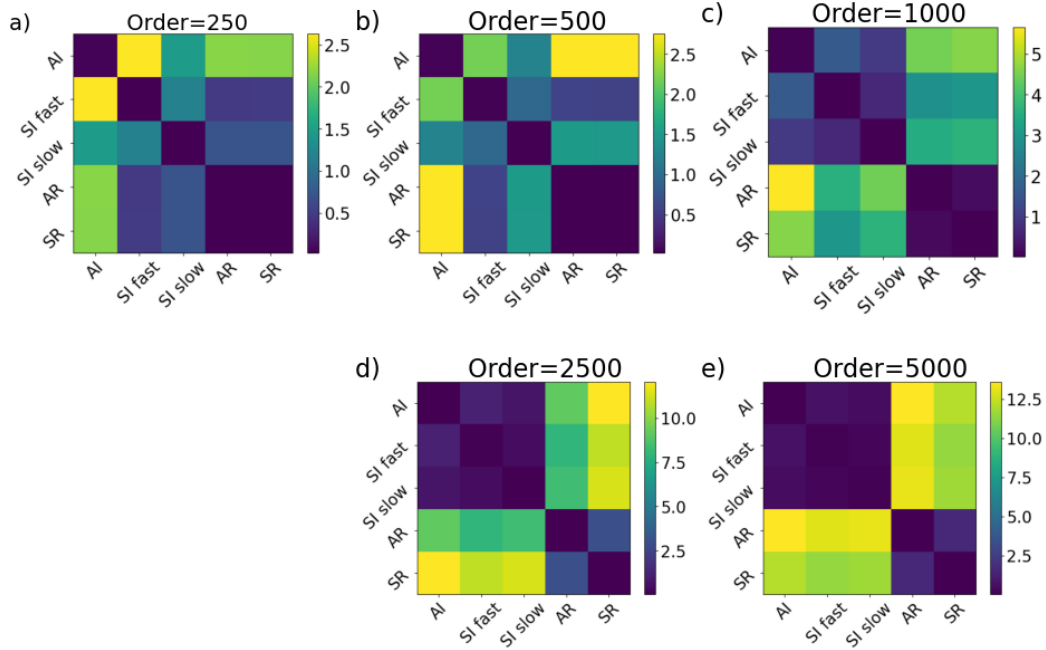
Figure 4.15: Wasserstein distances between the different regimes using the delta synapse model. Figure a) shows the Wasserstein distances for networks of size 250, b) shows the Wasserstein distances for networks of size 500, c) shows the Wasserstein distances for networks of size 1000, d) shows the Wasserstein distances for networks of size 2500, e) shows the Wasserstein distances for networks of size 5000.

The heatmaps representing the Wasserstein distances between the regimes using the alpha synapse model are showed in figure 4.16. We see that the Wasserstein distances are larger for the alpha synapse model compared to the delta synapse model in all network sizes. As we observed in figure 4.13, the alpha synapse seems to fire at a maximum possible firing rate in the regular regimes with very small coefficient of variation and very high correlation coefficient for all network sizes, leading to very small Wasserstein distances between these two regimes. This firing behavior is not observed in the irregular regimes, so the observed Wasserstein distances between the regular and irregular regimes become very large. Within the irregular regimes, we see that the Wasserstein distances between these regimes are quite high in the smaller networks, but these distances tend to become smaller as the size of the networks increase. We also observe that for each irregular, the within-regime Wasserstein distances are quite high in the smaller sized networks, meaning that there is a lot of variability displayed in the dynamics within each regime.

This within-regime variability declines as the size of the network increase, and for the network with size 5000, the within-regime variability is dropping to the levels observed in the regular regimes. For all network size the largest Wasserstein distance observed is between the asynchronous irregular regime and the regular regimes.
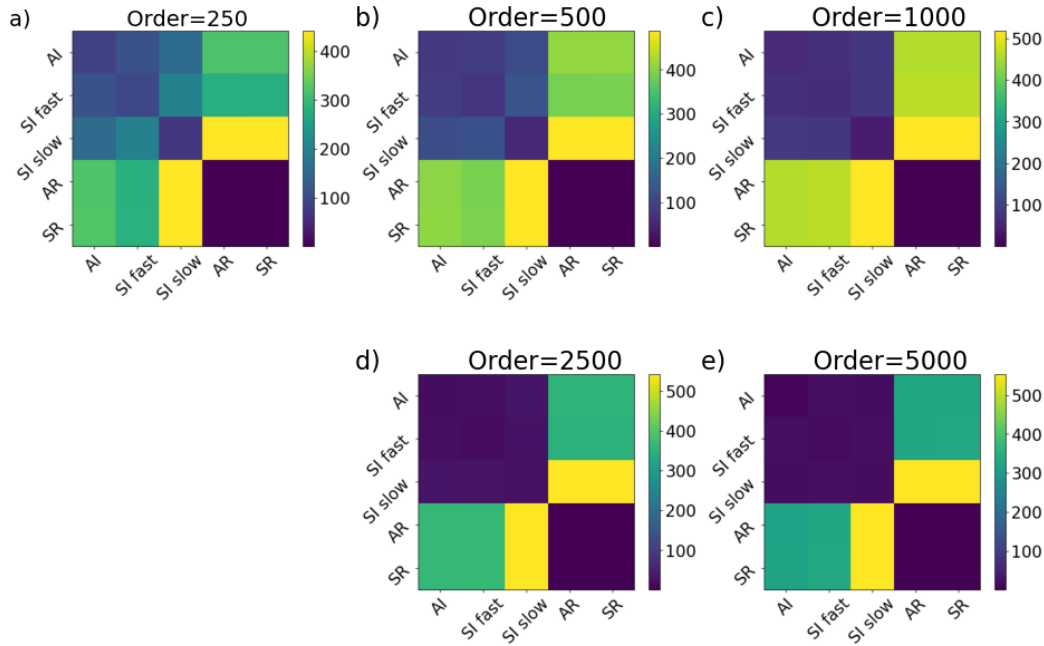
Figure 4.16: Wasserstein distances between the different regimes using the alpha synapse model. Figure a) shows the Wasserstein distances for networks of size 250, b) shows the Wasserstein distances for networks of size 500, c) shows the Wasserstein distances for networks of size 1000, d) shows the Wasserstein distances for networks of size 2500, e) shows the Wasserstein distances for networks of size 5000.

In the heatmaps showing the Wasserstein distances for the exponential decay synapse model, figure 4.17, the slow oscillating synchronous regime have been removed since there is no firing in this regime. Including this regime would add large Wasserstein distances too each plot, making the other Wasserstein distances very small, lowering the interpretability of the heatmaps. From the heatmap we see that the within-regime Wasserstein distances are low for all regimes across all network sizes. For the networks of size 1000 and below we observe that the Wasserstein distance is the largest between the asynchronous irregular and fast oscillating synchronous irregular regime, while the Wasserstein distance is low between the regular regimes. The distance is also low be-

tween the regular regimes and the fast oscillating synchronous irregular regime. It is also somewhat low between the asynchronous irregular regime and regular regimes. When the size of the network is over 1000, we see that the Wasserstein distance between the regular and irregular increase. The distances between the irregular regimes appear to stay around the same value when the network size is over 1000, and the separation between the regular and irregular regimes are dominating the networks of size 2500 and 5000. When the network reach size 5000, we observe very large Wasserstein distances between the asynchronous regular regime and the irregular regime. This distance is getting close to the Wasserstein distances observed in with the alpha synapse. Interestingly, the Wasserstein distance between the regular regimes gets quite large when the network is of size 5000. This pattern is also present for the delta synapse, but the Wasserstein distances are only around 5 for the delta synapse, whereas for the exponential synapse the Wasserstein distance between these regimes are around 100.
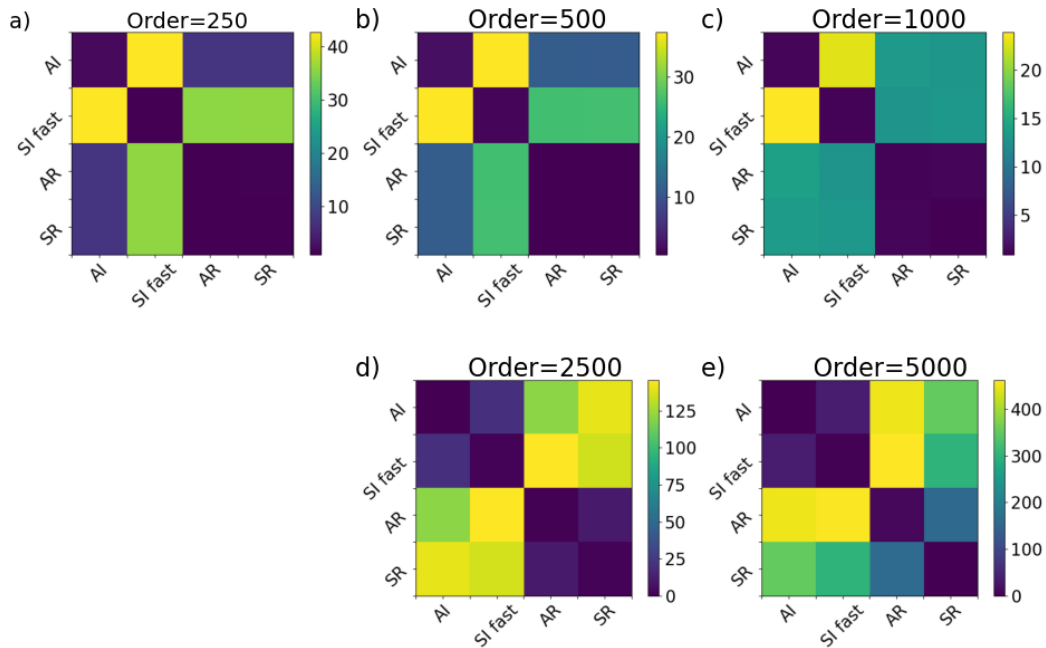
Figure 4.17: Wasserstein distances between the different regimes using the exponential decay synapse model. Figure a) shows the Wasserstein distances for networks of size 250, b) shows the Wasserstein distances for networks of size 500, c) shows the Wasserstein distances for networks of size 1000, d) shows the Wasserstein distances for networks of size 2500, e) shows the Wasserstein distances for networks of size 5000.

Chapter 5

Discussion

The key findings for this thesis, presented in the previous section, is that we can see clear differences in the dynamics observed in networks of neurons where we use the delta, alpha and exponential decay functions to model the synapse. We also observed that changing the network size had an effect on the dynamics in the network, and that this effect was different for the different regimes. In addition, we observed that the dynamics within each regime were not constant, and that the observed values for the firing rate, coefficient of variation, and correlation coefficient could vary within certain regimes. The variation observed in these metrics between some of the regimes were in some cases less than the variation we observed within some regimes, leading us to believe that the differences between certain regimes may not be as clear cut as in Brunel (2000).

5.1   The different synapse models

We presented the dynamics observed in all regimes for the different synapse models in table 4.1, showing the spiking statistics, and in table 4.2, showing the Wasserstein distances. The most evident differences we observed were in firing rate, and Wasserstein distances. For these metrics, the separation between the different synapse models is clear in all regimes. The alpha synapse model shows the highest firing and the largest Wasserstein distances in all regimes. The exponential decay synapse model displays the lowest firing rates and the smallest Wasserstein distance in all regimes, and the delta synapse model falls

in between on both metrics in all regimes.

Using the coefficient of variation, the irregular regimes stand out for the alpha synapse, where the coefficient of variation is an order of 10 higher than for the other two synapse models. This makes us believe that the alpha synapse model is operating in a different regime than the other two synapse models for these parameter settings. For the delta and exponential decay model the coefficient of variation is of the same order, and the observed values are similar, making it hard to separate these synapse models based on this metric in the irregular regimes. In the regular regimes, the coefficient of variation is 0 or close to 0, making it impossible to separate the synapse models in these regimes based on this metric alone.

The differences in the correlation coefficient are quite evident in the regular regimes where it is very high for the alpha synapse model. In the synchronous regular regime, the correlation coefficient is lower than the in the synchronous irregular regime for both the delta synapse model and the exponential decay synapse model, and the in both regimes the lowest correlation coefficient is observed in the exponential decay synapse model, making it possible to differentiate between all the synapse models using this metric in the regular regimes. In the irregular regimes, all the correlation coefficients are of the same order, and very close to each other in value, making any possible differentiation between the synapse models impossible in these regimes. The one exception is the exponential model in the slow oscillating synchronous irregular regime, where there is no firing observed in the network, making all spiking statistics, including the correlation coefficient, 0.

For the delta model, the activity in the slow oscillating synchronous regime is also very low, with an average firing rate of 1.32 spikes per second. Different from the other synapse models, the alpha synapse model displays relatively high activity in this regime, with a firing rate higher than what is observed in the asynchronous irregular regime using the other synapse models. In the regular regimes the alpha synapse model is firing with a firing rate of 476.25 spikes per second, with negligible standard deviation. The coefficient of variation is 0 in these regimes, and the correlation coefficient is very high. The maximum possible firing rate in our model is 500 spikes per second. We have a fixed refractory period set to 2 ms, making 500 spikes per second the maximum possible firing rate. The alpha synapse model is getting close to this ceiling in

the regular regimes.

When we attempted to make the alpha and exponential decay synapse models display similar dynamics to the delta synapse, we found it very difficult to bring the firing rate of the alpha synapse down in the regular regimes. For all sets of parameters we tried, the neurons were still firing at rates above 470 spikes per second, as displayed in 4.4. In the irregular regimes, we were able to get the dynamics of the alpha synapse model closer to that of the delta synapse model. For the exponential decay synapse, we were able to recreate the dynamics of the delta synapse model quite well in all regimes. We were able to introduce neuron firing in the slow oscillating irregular regime which originally displayed no neuron firing.
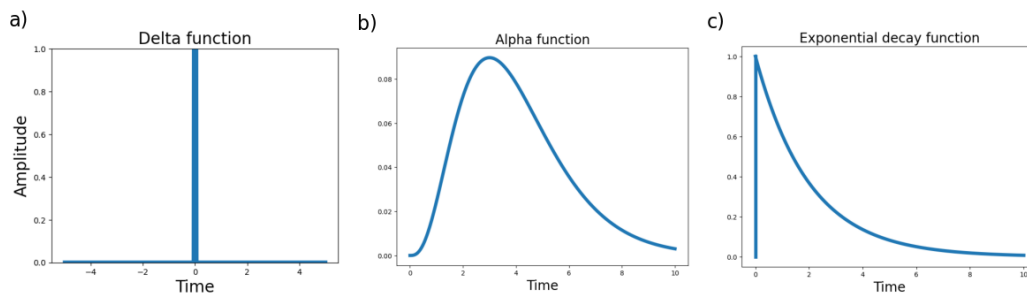
Figure 5.1: The curve produced by a) the delta function, b) the alpha function, and c) the exponential decay function.

To summarize the observations between the different synapse models, we can clearly see that there is a difference in the dynamics displayed by the different synapse models. We believe this to mainly be an effect of the total current that the different synapse models inject into the postsynaptic neurons. The curves produced by the different synapse models are shown in shown in figure 5.1. The area under the curve represents the total current in the synapse. When taking the integral over the same interval, the alpha function has the largest area, and the exponential decay function has the smallest area under

the curve. It is not possible to integrate the delta function on an interval, but the area under the curve for the delta function is defined to be 1, as given in equation 2.10.

5.2 The synapse models in networks of different sizes

The observation that the neuron firing in the regular regimes using the alpha synapse model appears to be stuck close to some ceiling seem to carry over to the simulations using networks of different sizes. From figure 4.16 we see that the firing rate is constantly around 476 spikes per second for all sized networks where we use the alpha synapse. The coefficient of variation is also close to 0 for all the different network sizes. We do observe some variation in the correlation coefficient, but it is generally high for all network sizes. In the irregular regimes, the firing rate is falling as the network size is increasing. Interestingly, the coefficient of variation is also falling as the network size is increasing. It is more common to observe an increase in the coefficient of variation as the firing rate is decreasing. However, we do observe the same trend for the alpha synapse in table 4.1. In this table, these observations are from different regimes, whereas the effect from different network sizes are from within-regime observations.

The delta- and exponential decay synapse models show a similar pattern in the irregular regimes, where the firing rate is falling as the size of the network is increasing. This is not true for the exponential decay synapse model in the slow oscillating synchronous irregular regime, where there is no firing for any sized network. As the firing rate is increasing, the coefficient of variation is increasing for both synapse models in all regimes, except for the delta synapse in the slow oscillating synchronous irregular regime, where both the firing rate and coefficient of variation are falling as the network size is increasing. However, this trend is not observed for a network of size 5000 with a delta synapse model, where the firing rate is falling, and the correlation of variation is increasing. In the regular regimes, the firing rate for both synapses are increasing as the network size is increasing, accompanied by a falling coefficient of variation. With a network of 5000, the delta synapse model in the asynchronous regular

regime has a large increase in the coefficient of variation.

From the heatmaps in figure 4.16 we see that the Wasserstein distances between the regular and irregular regimes are high for all network sizes in all three synapse models, except for networks of size 1000 and below using the exponential decay model, and the network of size 250 using the delta synapse model, where the largest Wasserstein distance is observed between the asynchronous and fast oscillating irregular regimes.

The effect changing the size of a network of neurons may have on the dynamics of a network has been explored in Albada et al. (2015). In general, their results showed an increase in the average activity of a network when the network size is increased. They reasoned that the main driver for this observation is that each neuron will receive synaptic input form a larger number of neurons when the network size is increased. In our work, we observed an increase in firing rate in the regular firing regimes. In the irregular firing regimes, our simulations displayed a decrease in firing rate as the network size was increased. As reported by Brunel (2000), excitatory neurons dominate the inhibitory neurons in the regular regimes, and in the irregular regimes the inhibitory neurons dominate the excitatory neurons. Increasing the size of the networks may amplify this effect because of the increase in synaptic input the neurons receive.

5.3 Exploration of the regimes

In figure 4.4 to 4.7 we explored selected areas within each regime from (Brunel, 2000). We observed that the spiking statistics were not uniform throughout the selected areas. The only uniform observations were seen for the exponential decay synapse model in the slow oscillating SI regime, and in the regular regimes for the alpha synapse. As previously mentioned, these regimes stand out as there is no firing in the slow SI regime observed for the exponential decay synapse model and that the firing in the regular regimes appear to hit a ceiling for the alpha synapse. In addition, the exponential decay synapse model did not have any firing observed in a lot of AI regime. We observed a difference in how the different synapse models varied within each regime, where the alpha synapse model displayed the highest variability in the irregular regimes, and

the lowest variability in the regular regimes. The exponential decay model displayed the lowest variability in the irregular regimes

When we take into account figure 4.9 - 4.11 there is a clear difference in the dynamics between the synchronous regime regular and the irregular regimes. But the differences between the irregular regimes does not appear to be as evident as reported in Brunel (2000). We did observe some difference in the dynamics displayed by the three different synapse models in these regimes. The alpha and the exponential decay synapse model displayed dynamics that did not suggest to us that there were clear lines that could be drawn between the irregular regimes. For the delta synapse model, we observed some differences between the AI regime and the slow oscillating SI regime, but the main difference was that the neuron firing stopped in certain parts of the slow oscillating SI regime. Between the AI and fast oscillating SI regime, the delta synapse model does not seem to display a clear boundary between the regimes.

Based on these observations it is difficult say that there exist clear boundaries between the different irregular regimes. The alpha and exponential decay synapse models do not necessarily operate in the same regimes as the delta synapse model for the same parameter combinations, but it is interesting that it is difficult to make the separation for all three synapse models in the irregular regimes. However, we need to take into account the different approach we have taken when creating the heatmaps showing the spiking statistics, and the approach that Brunel has taken. Brunel made the borders between the regimes based on calculations of Hopf bifurcation lines. The procedure used in this paper is described in detail in the appendix A in Brunel (2000). The figures we made are based on the experimental results from our simulations. There may be some effects present in our simulations that was not taken into account in the calculations made by Brunel. However, we would have like to see a clearer separation between the irregular regimes in figure 4.10, as reported by Brunel.

5.4 Conclusion

The main finding of this thesis is that using different waveform functions, the delta, alpha and exponential decay function, to model the synapse between neurons will result in different dynamics being displayed in a network of neu-

rons. We found that the alpha synapse resulted in the highest rate of neuron firing in all firing regimes and in networks of all sizes. In the regular firing regimes, the alpha synapse got close to the maximum firing rate that is possible in our model, due to the 2 ms refractory period. It was difficult to lower the firing rate for the alpha synapse in these regimes by varying neuron parameters. The exponential decay function displayed the lowest firing rate in all firing regimes and in all network sizes, and the firing rate of the delta function lied in-between in all regimes and all network size. The observed change in dynamics were similar for the three different synapse models in response to changing the size of the network. In the regular regimes, increasing the network size led to an increase in the firing rate, while in the irregular regimes the firing rate decreased as the size of the network was increased. Our results from sweeping over selected areas in from figure 2 in Brunel (2000) indicate that the differences between the irregular firing regimes may not be as clearly identified as suggested by Brunel, but we are careful to not make a bold conclusion about this. In the future it would be interesting to explore whether using a different approach to recalculate the synaptic weights when using the alpha synapse may lead to different results. Especially, it would be interesting to explore whether it is possible to bring down the very high firing rate displayed by the alpha synapse in the regular firing regimes. It could also be interesting to explore whether we could find a method to recalculate the synaptic weights in order to decrease the change in neuron activity we observed for all three synapse models in differently sized networks.

References

Abbott, L. F. (1999). Lapicque's introduction of the integrate-and-fire model neuron (1907). *Brain Research Bulletin*, 50:303–304.

Albada, S. J., Helias, M., and M., D. (2015). Scalability of asynchronous networks is limited by one-to-one mapping between effective connectivity and correlations. *PLOS Computations Biology*, pages 1–37.

Bloom, F., Nelson, C. A., and A., L. (2005). *Brain, Mind, and Behavior*. Educational Broadcasting Corporation, US, 3rd edition.

Brunel, N. (2000). Dynamics of sparsely connected networks of excitatory and inhibitory spiking neulrons. *Journal of Computational Neuroscience*, 8:183–208.

Corless, R. M., Gonnet, G. H., Hare, D. E. G., Jeffrey, D. J., and Knuth, D. E. (1996). On the lambert w funciton. 5:329–360.

Dayan, P. and Abbott, L. F. (2001). *Theoretical Neuroscience - Computational and Mathematical Modeling of Neural System*. MIT Press, Mass, US, 1st edition.

Devore, J. L., Berk, K. N., and Carlton, M. A. (2021). *Modern Mathematical Statistics with Applications*. Springer Nature, Switzerland, 3rd edition.

Eppler, J. M., Helias, M., Muller, E., Diesmann, M., and Gewaltig, M. O. (2009). Pynest: A convenient interface to the nest simulator. *Frontiers in Neuroinformatics*, 2(12):1–12.

Gabbani, F. and Koch, N. (1998). *Methods in Neuronal Modeling: From Ions to Networks*. MIT Press, Mass, US, 2nd edition.

Garcia, S., Guarino, D., Jailet, F., Jennings, T., Propper, R., Rautenberg, P. L., C., R. C., Sobolev, A., Wachtler, T., P., Y., and P, D. A. (2014).

Neo: an object model for handling electrophysiology data in multiple formats. *Frontiers in Neuroinformatics*, 8(10):1–10.

Hodgkin, A. L. and Huxley, A. F. (1952). Currents carried by sodium and potassium ions through the membrane of the giant axon of loligo. *J. Pysiol*, 116:449–472.

Kanwal, R. P. (1983). *Generalized Functions: Theory and Technique*. Academic Press, New York, US, 1st edition.

Krishnan, J., Prota Mana, P. G. L., Helias, M., Diesmann, M., and Di Napoli, E. (2017). Perfect spike detection via time reversal. *Frontiers in Neuroinformatics*, 11):1–35.

Matplotlib (2021). matplotlib.colors.powernorm. Accessed: 2022-05-08.

Mezentsev, P. (2020). Jusuf – new multi-purpose computing platform for neuroscientists. Accessed: 2023-29-04.

POT (2021). Pot:python optimal transport. Accessed: 2022-04-21.

Python Software Foundation (2023). concurrent.futures - launching parallel tasks. Accessed: 2022-05-07.

Rall, W. (1967). Distinguishing theoretical synaptic potentials computed for different somadendritic distributions of synaptic inputs. *Journal of Neuropysiology*, 30:1138–1168.

Ramdas, A., Trillos, N. G., and Cuturi, M. (2017). On wasserstein two-sample testing and related families of nonparametric tests. *Entropy*, 19(2):1–15.

Rotter, S. and Diesmann, M. (1998). Exact digital simulation of time-invariant linear systems with applications to neuronal modeling. *Biological Cybernetics*, 81:381–402.

Scipy (2023). scipy.stats.wassersteindistance. Accessed: 2022-05-05.

Sinha, A., de Schepper, R., Pronold, J., Mitchell, J., Mørk, H., Nagendra Babu, P., Eppler, J. M., Lober, M., Linssen, C., Terhorst, D., Benelhedi, M. A., Morrison, A., Wybo, W., Trensch, G., Deepu, R., Haug, N., Kurth, A., Vennemo, S. B., Graber, S., Spreizer, S., Gille, J., Vogelsang, J., Krüger, M., and Plesser, H. E. (2023). Nest 3.4.

Sterratt, D., Graham, B., Gillies, A., and Willshaw, D. (2011). *Principles of Computational Modelling in Neuroscience.* Cambridge Univeristy Press, Cambridge, UK, 1st edition.

Wnuk, A., Davis, A., Parks, C., Halber, D., Kelly, D., Zyla, G., Hopkin, K., Weintraub, K., Beverly, J. M., Sheikh, K. S., Wessel, L., Chiu, L., Fessenden, M., Galinato, M., Richardson, M., Blumenrath, S., and Rojahn, S. (2018). *Brain Facts, a primer on the brain and nervous system.* The Society of Neuroscience, Washington DC, US, 8th edition.

Yegenoglu, A., Denker, M., and Grün, S. (2018). Collaborative hpc-enabled workflows on the hbp collaboratory using the elephant framework. *Neuroinformatics*, page P19.